Electronic Supplementary Material (ESI) for Physical Chemistry Chemical Physics.

Supporting Information for

Structural Inhomogeneity as a Factor Promoting the Homogenous Catalysis of CO_2 Hydrogenation by $(PMe_3)_4RuH_2$

Guang-Jie Xia[1], Jianwen Liu[2], and Zhi-Feng Liu[1,*]

[1]Department of Chemistry and Centre for Scientific Modeling and Computation

Chinese University of Hong Kong, Shatin, Hong Kong, China

and

[2] College of Materials Science and Engineering, Shenzhen University,

Shenzhen, China

*****To whom correspondence should be addressed. Email: zfliu@cuhk.edu.hk fax: ++852-2603-5057

Content:

Cartesian coordinates of the intermediates and transition states are provided in "XYZ_Coordinates.txt".

Please contact the corresponding author if a reader would like to examine the AIMD trajectory files.

1. Tests on solvation corrections and dispersion corrections.

To evaluate the solvation effect of the CO_2, the integral equation formalism of the polarizable continuum model (IEFPCM) is applied on the gas-phase optimized geometries of complexes. As shown in the Table S1, in the first way, the n-heptane is used to mimic the hydrophobic environment of $scCO_2$, as suggested by the previous studies[1,2]; in the second way, a similar solvent, carbon disulfide is used with the dielectric constant replace by the value of the $scCO_2$ (ε=1.49)[3]. In both ways, the changes of the complex relative energies are in most cases smaller than 1 kcal/mol leading to even smaller changes on the corresponding reaction barriers, which implies the solvation effect does not have a strong influence on the energies, because the solvent CO_2 molecule is basically nonpolar.

Table S1: Comparison on the relative energies and that corrected by the Polarizable Continuum Model using the integral equation formalism variant (IEFPCM) and D3 dispersion correction. All energies are calculated by the B3LYP functional.

Relative Energy (in kcal/mol)	E_{ZPC}	$E_{ZPC+PCM}$[a]	$E_{ZPC+PCM}$[b]
C1a	0.0	0.0	0.0
CW-C1a	15.7	16.0	15.9
C1aW	-5.7	-4.7	-4.9
$TS_{C2aW-C3aW}$	12.6	9.7	10.7
C4aW	-12.9	-12.8	-12.9
$TS_{C4aW-T4bW}$	-0.8	-0.5	-0.6
T4bW	-5.3	-4.6	-4.8
$TS_{T4bW-T4cWN}$	3.7	4.0	4.0
$T4cW_N$	-8.5	-8.8	-8.6
$TS_{T4dWRp-T4dNWRp}$	8.2	9.3	8.9
$T4dNW_{Rp}$	0.4	1.2	1.0

[a] n-heptane as the solvent is used to mimic CO_2. [b] Carbon disulfide is used with the dielectric constant replace by the value of the $scCO_2$ (ε=1.49)..

Dispersion corrected B3LYP (B3LYP+D3) is also tested with some typical reaction steps. The results are shown in Table S2.

For the unimolecular reactions, the reaction energies and barriers calculated by B3LYP, B3LYP+D3, PBE0 and M06 are very similar. For example, in the HCOO rotation step with one water around, all the reaction energies and barriers calculated by different methods are in most cases within the differences in 2 kcal/mol, except a

relatively smaller barrier calculated by B3LYP+D3. For the crucial H_2 metathesis step, which locates between TDI and TDTS, the reaction energies are also similar within 11.5~13.0 kcal/mol. The barriers by B3LYP and PBE0 are quite similar with 13.6 and 13.0 kcal/mol respectively, while the barrier by B3LYP-D3 is slightly smaller and that by M06 slightly larger.

For bimolecular step which involves PMe_3 ligand insertion or disassociation, B3LYP shows considerably smaller reaction energy change. This may come from the underestimation of Ru-P binding energy with B3LYP, which is also observed in the precious benchmark study[4]. By applying D3 correction, the results can accord with that by PBE0 and M06. This suggests the D3 correction is needed when B3LYP is used in those reaction steps with ligand changes. As shown in Table S2, the Ru-PMe_3 binding energies are close for B3LYP-D3 and PBE0 functionals, while with the discussion in the paper, the B3LYP and PBE0 results actually lead to the same conclusion despite of the underestimation of B3LYP in these binding energies. In previous theoretical studies of the CO_2 hydrogenation in $scCO_2$, [1,2] the dispersion correction is not involved. Considering the PBE0 functional is already implemented throughout the calculation, to have a better comparison with the previous computational result[1,2], B3LYP is discussed in the paper and B3LYP-D3 is only tested in this work.

Table S2: Comparison on the reaction energies and barriers calculated by B3LYP, B3LYP with dispersion correction on D3 level, PBE0 and M06 functional.

Reaction Energy & Barrier (in kcal/mol)	B3LYP ΔE (E_a)	B3LYP-D3 ΔE (E_a)	PBE0 ΔE (E_a)	M06 ΔE (E_a)
Unimolecular Step:				
HCOO rotation step: $(PMe_3)_4RuH(HCOO)\cdot(H_2O)$ $\rightarrow(PMe_3)_4RuH(OHCO)\cdot(H_2O)$ [C2aW→C3aW]	-11.8 (12.6)	-10.9 (6.3)	-11.0 (12.6)	-10.2 (10.3)
H_2 metathesis step: $(PMe_3)_3RuH(H_2)(OHCO)\cdot(H_2O)$ $\rightarrow(PMe_3)_3RuH_2(OHCOH)\cdot(H_2O)$ [$T4cW_{Rp}$→$T4dW_{Rp}$]	+12.1 (13.6)	+11.5 (11.2)	+11.8 (13.0)	+13.0 (15.4)
Bimolecular Step:				
Intramolecular ligand disassociation: $(PMe_3)_4RuH(OHCO)\cdot(H_2O)$ $\rightarrow(PMe_3)_3RuH(\eta^2\text{-}OOCH)\cdot(H_2O)+ PMe_3$ [C4aW→T4bW+PMe_3]	+7.6 (12.1)	+11.5 (17.8)	+15.4 (19.0)	+17.5 (13.9)
Formation of water coordinated complex: $(PMe_3)_4RuH_2)+H_2O$ $\rightarrow(PMe_3)_3(H_2O)RuH_2+ PMe_3$ [C1a+ H_2O→CW-C1a+PMe_3]	+15.7 (---)	+25.3 (---)	+23.6 (---)	+26.7 (---)

2. Supplementary AIMD result

According to the experimental data of high-pressure CO_2 (120 bar) and H_2 (80 bar), [5] the density of CO_2 and H_2 is 11.60 mol/L and 2.88 mol/L respectively. For the solute of different Ru complex with 2, 5 or 8 waters, and one PMe_3 in some cases, the total solvation solvent-excluded molecular volume is estimated to be 380~600 $Å^3$. Within a 20Å·20Å·20Å cubic box, the left volume corresponds to 52 or 53 CO_2 and 13 H_2. Hence in the AIMD calculation, we implement 53 CO_2 and 13 H_2 to mimic the supercritical environment with 120 bar CO_2 and 80 bar H_2 in experiment.

2.1 $(PMe_3)_4RuH_2$ (C1a) with 5 H_2O at 423.15K.

Besides the AIMD reported in Figure 2, which is done at the experimental temperature, 323.15K, we also implemented the AIMD calculation of the same solute at 423.15K. As the higher temperature, the first solvation shell still remains the same with a peak around 3.8 Å and consists two water molecules, as shown in Figure S1(a). With the more active thermal motion, the edge of the first solvation shell slightly extends outward to 4.8 Å, and the more frequent exchange between the two solvation shells is observed.

The RDF of CO_2, which is introduced as the solvent in the AIMD, is also under statistics in Figure S1(b). It is obvious, in the range of the first solvation (< 4.8 Å), the distribution of CO_2 is very low. This implies there is no strong interaction between CO_2 and the hydrophilic active site of the complex because CO_2 is nonpolar and hydrophobic. This is accord with the observation that CO_2 insertion is a collision process in our previous paper.[6] This is the case of $(PMe_3)_4RuH_2$ with 5 H_2O at 423.15K. In fact, for different AIMD at 323.15K, similar RDF curves of CO_2 are observed, which indicates no strong interaction between CO_2 and Ru complex.

Although CO_2 does not have any strong interaction with the Ru complex, within the Ru-C distance of 4 Å still very few CO_2 are distributed. Considering the Ru-C distance in the CO_2 insertion transition state ($TS_{C1aW\text{-}C2aW}$) is ~3.4 Å, this implies even with the water surrounded, although hard, the CO_2 still have the chance to attack the hydride on Ru to insert into the complex, because of its small molecule scale and high concentration.

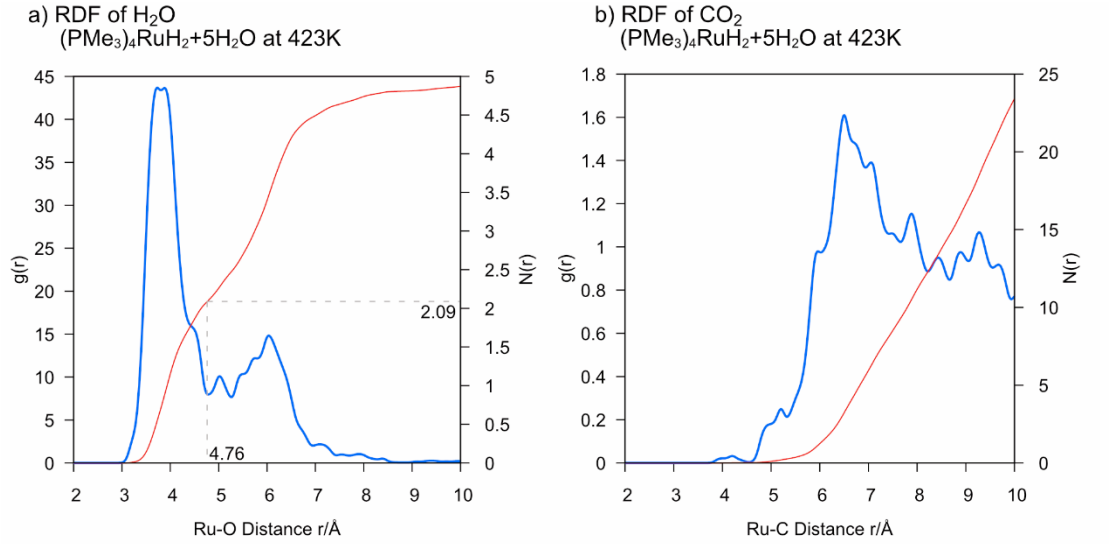

Figure S1: AIMD simulation on $(PMe_3)_4RuH_2$ with 5 H_2O, 53 CO_2 and 13 H_2 molecules at a higher temperature of 423.15K. a) The radial distribution functions g(r) (RDF) of the O atoms on H_2O around the Ru center. b) The radial distribution functions g(r) (RDF) of the C atoms on CO_2 around the Ru cente. The left y-axis is for g(r) (the blue curve), while the right y-axis is for the integrated number of O or C atoms (the red curve).

2.2 $(PMe_3)_3RuH(\eta^2\text{-}OOCH)$ (T4b) with 5 or 8 H_2O

Considering the intramolecular ligand disassociation is the crucial step in the catalytic cycle of $(PMe_3)_4RuH_2$ without and additives, the AIMD with $(PMe_3)_3RuH(\eta^2\text{-}OOCH)$ (T4b) with 5 or 8 H_2O is also done at 323.15K. As shown in Figure S2(b), different from the case of $(PMe_3)_4RuH_2$ in Figure 3 and $(PMe_3)_3RuH_2(OCH\text{-}OH\cdot NMe_3)$ in Figure 7, no obvious first solvation shell is shown here, in spite of a very large and broad peak on RDF from 3 to 5 Å. That is because the two O atoms on the bidentate OOCH ligand is quite hydrophilic and can be easily boned with waters. The waters originally in the outer solvation shell is attracted inside to merge with the first solvation shell.

Almost no chemical reaction is observed in our AIMD calculations, except the system of T4b with 5 H_2O, as shown in Figure S2(a). After the equilibrium of the initial 5 ps, at around 6.8 ps the $(PMe_3)_3RuH(\eta^2\text{-}OOCH)$ complex (T4b) can transfer to $(PMe_3)_3(H_2O)RuH(OCHO)$ with a water insertion. This reaction lead to a sharp peak of RDF curve at around 2.3 Å. That is the coordinated water molecule. The integration of that is 0.88, because in the first 12% time(1.8ps of the total 15ps), this water is still not inserted. In fact, this water insertion reaction here is the reverse reaction from CW-C3a to T4bW in Figure 8. In the reaction CW-C3a to T4bW, the E_a

is only 0.1 kcal/mol in B3LYP and 1.3 kcal/mol in PBE0; while the reverse reaction is also easy to happen with the E_a of only 0.9 kcal/mol in B3LYP and 3.6 kcal/mol in PBE0. The thermal energy of 323K in the AIMD can overcome such a small barrier to make the reaction happen. However, what should be paid attention here is the reaction in AIMD is highly accidental even with such small barriers. In the AIMD with 8 waters, no formation of water coordinated structure is observed. At a large timescale, it is expected this reaction can also happen with 8 or more waters and in the case of 5 waters the coordinated water can be substituted back to the η^2-OOCH, but the computational cost is too high at the stage.

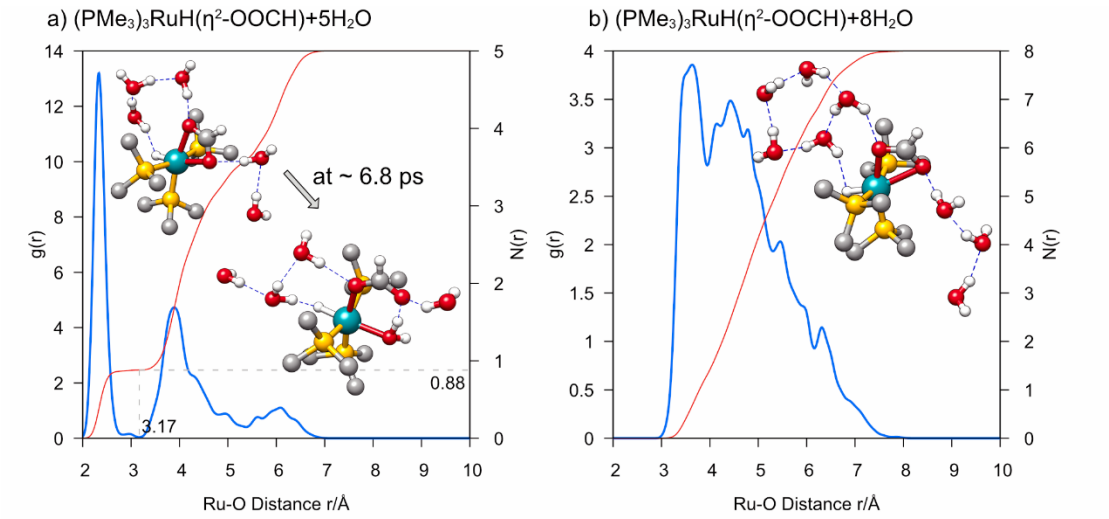

Figure S2: The radial distribution functions *g(r)* (RDF) of the O atoms of H_2O around the Ru center. (a) $(PMe_3)_3RuH(\eta^2\text{-}OOCH)$ (T4b) + $5H_2O$; (b) $(PMe_3)_3RuH(\eta^2\text{-}OOCH)$ (T4b) + $8H_2O$. The left y-axis is for *g(r)* (the blue curve), while the right y-axis is for the integrated number of O atoms (the red curve). The structure shows the typical conformation the MD trajectory.

2.3 $(PMe_3)_3(H_2O)RuH_2$ (CW-C1a) with 1, 4 or 7 H_2O and one extra PMe_3

After the competition of in the ligand substitution of the $HCOOH{\cdot}NMe_3$ elimination, although energetically the $(PMe_3)_4RuH_2{\cdot}(H_2O)$ is the favorable product, the actual product is the $(PMe_3)_3(H_2O)RuH_2$ driven by dynamic effect of water molecules solvated around the complex, which has been extensively discussed in Section 3.3. However, after the formation of $(PMe_3)_3(H_2O)RuH_2$, there still exists a possibly that one free PMe_3 can substitute the coordinated water out to form $(PMe_3)_4RuH_2{\cdot}(H_2O)$ again, because the later one has a considerable lower relative energy. In the case of $(PMe_3)_3(H_2O)RuH_2$ with 1 H_2O, the calculated free energy barrier is only 2.9 kcal/mol, which seems apparently feasible. To investigate this

reaction, the AIMD of $(PMe_3)_3(H_2O)RuH_2$ (CW-C1a) with 1, 4 or 7 H_2O and one extra PMe_3 is done, as shown in Figure S3.

In the case of one additional water, the added water binds with both the formal one and the hydride. Both waters are stable in position, and two sharp peaks on RDF curve are observed. With 4 additional waters, the exchange between the coordinated water and the closest additional water is observed, which leads to average 0.87 water in the coordination shell. However, this ligand substitution only happens between the near waters, and the product and react are the same in this transformation. The free PMe_3 is quite far from the water cluster. When the water is added to 7, the coordinated water becomes stable again, and no water-water substitution happens. As the coordinated water itself is a hydrophilic molecule, besides the coordination shell, the remaining waters will aggregate around the coordinated water and the two hydride ligands, which forms a hydrophilic shell protecting the coordinated water.

As shown in Figure S3(d), in general when more waters are involved, the free PMe_3 is excluded outside. Occasionally the PMe_3 can reach a position "close" to Ru (5-6 Å) in the case of 7 waters, because of the interspace of water clusters. It is far from coordinated Ru-P distance or Ru-O distance, which is around 2.3 Å. The situation is different for CO_2, which is a smaller molecule and has large concentration. As shown in Figure S3(e), the RDF of CO_2 still have a value smaller than 4 Å. This distance is enough for CO_2 to attack the hydride on Ru, as in the CO_2 insertion transition state the Ru-C distance is around 3.4 Å. With the small barrier for CO_2 insertion into $(PMe_3)_3(H_2O)RuH_2$, with the protest of the water cluster, the $(PMe_3)_3(H_2O)RuH_2$ will dynamically undergo a CO_2 insertion rather than PMe_3 substitution reaction.

In addition, if we compare Figure S3(e) and Figure S1(b), it is not hard to find that the CO_2 RDF of $(PMe_3)_3(H_2O)RuH_2$ is much larger than that of $(PMe_3)_4RuH_2$ in the Ru-C distance range below 4 Å, although 2 more waters are surrounded. This shows a higher CO_2 insertion probability of $(PMe_3)_3(H_2O)RuH_2$, which accords with its lower CO_2 insertion barrier.

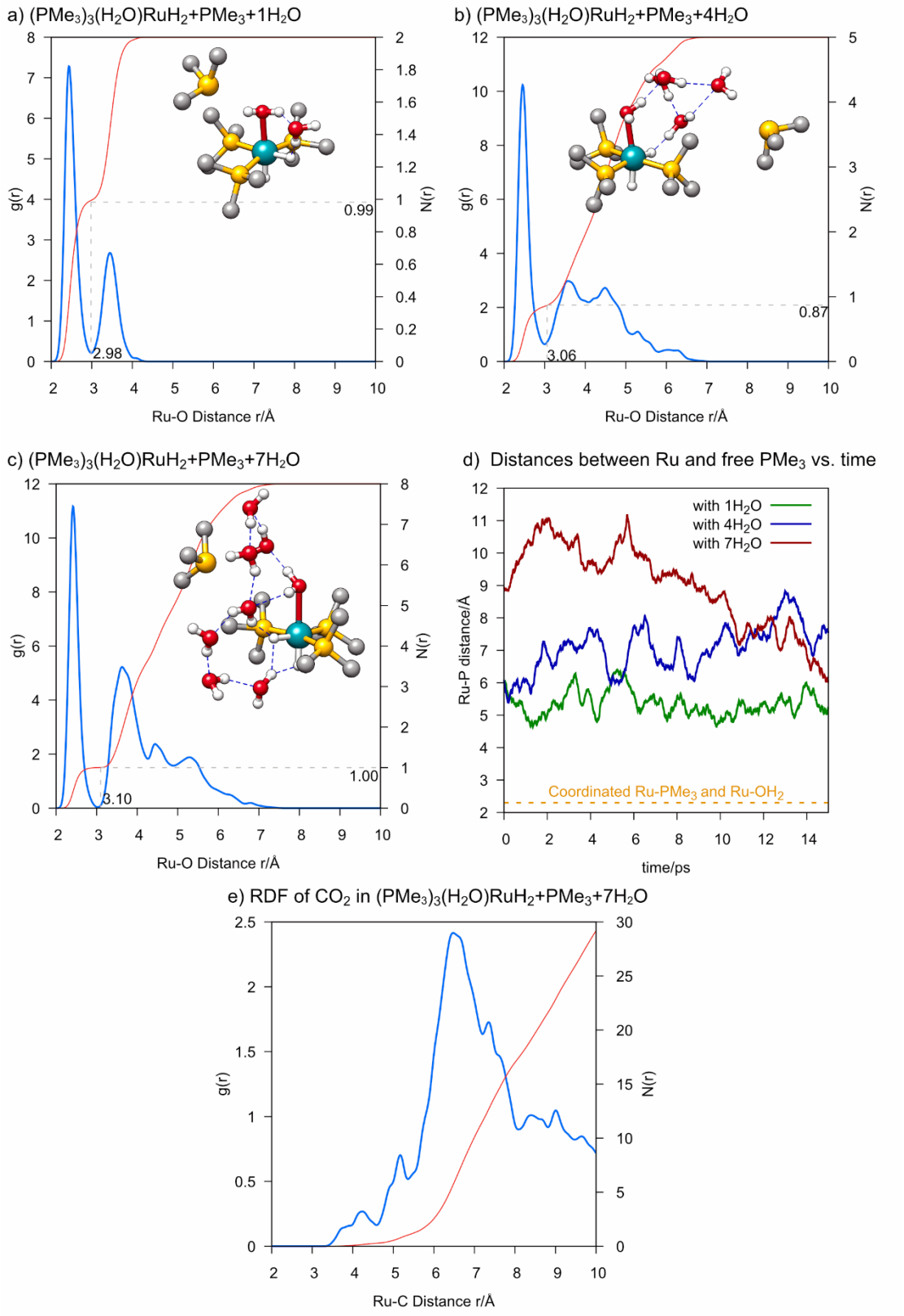

Figure S3: AIMD simulation on $(PMe_3)_3(H_2O)RuH_2$ with one extra PMe_3, several waters, 53 CO_2 and 13 H_2 molecules. a) 1 water; b) 4 waters; c) 7 waters: The radial distribution functions *g(r)* (RDF) of the O atoms on H_2O around the Ru center, with the left y-axis for *g(r)* (the blue curve) and the right y-axis for the integrated number

of O atoms (the red curve). The structure shows the typical conformation in the MD trajectory. d) The distance between Ru and the P atom on the free PMe_3 molecule vs. time. e) The RDF of the C atoms on CO_2 around the Ru center in the case of 7 waters.

3. Free Energy Values

The ΔG (including vibrational, translation and rotational entropy) and ΔG_{vib} (including vibrational entropy only) values along the reaction path in Figure 8 and Figure 9 is shown in Figure S4. For convenience, the $(PMe_3)_3RuH_2(H_2O)\cdot(H_2O)$, *i.e.* CW-C1aW, is taken as the reference of the free energy here. Similar discrepancy between ΔG and ΔG_{vib} is observed comparing to that in Figure 7.

Table S3 also provide all the calculated ΔG and ΔG_{vib} for the reaction paths discussed in both text and supporting information below.

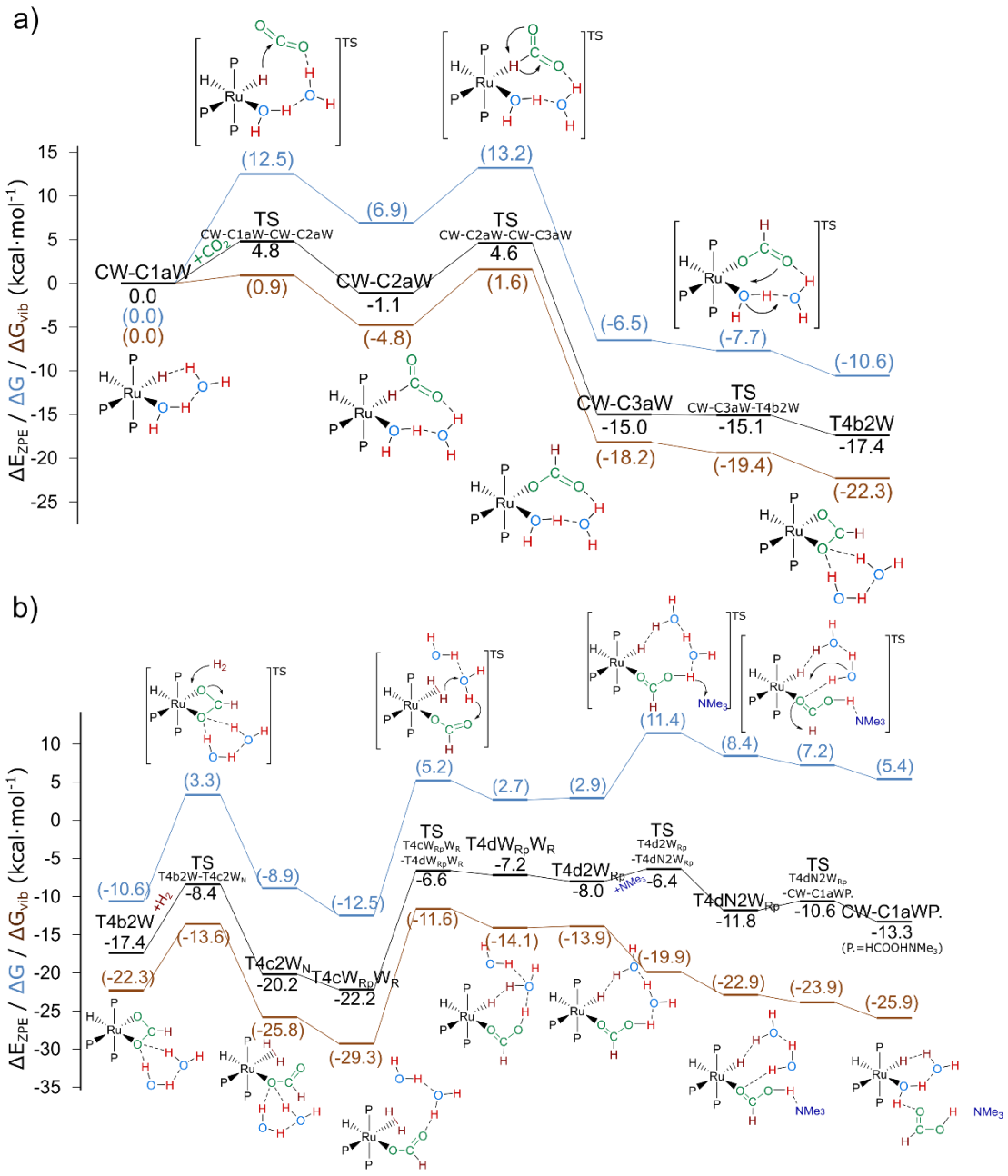

Figure S4: The relative energy (ΔE), Gibbs Free Energy (ΔG) and Gibbs Free Energy with only vibrational frequency involved (ΔG_{vib}) of the reaction pathway of $(PMe_3)_3RuH_2(H_2O)$ in the presence of a solvent H_2O. a) and b) corresponds to Figure 6 and 7 in the paper respectively. For convenience, the $(PMe_3)_3RuH_2(H_2O)\cdot(H_2O)$, *i.e.* CW-C1aW is taken as the reference of the free energy here.

Table S2: The relative energy(ΔE), relative Gibbs Free energy(ΔG) and relative Gibbs Free energy with only vibrational movements(ΔG_{vib}) of the complexes in the paper and supporting information.

Relative Energy/ Gibbs Free Energy (in kcal/mol)	**B3LYP**			**PBE0**		
	ΔE	ΔG	ΔG_{vib}	ΔE	ΔG	ΔG_{vib}
Reference: **C1a***	0.0	0.0	0.0	0.0	0.0	0.0
C1aW	-5.7	1.5	-8.2	-7.0	-0.5	-10.3
$TS_{C1aW-C2aW}$	0.0	14.6	-6.7	-1.9	13.4	-7.9
C2aW	0.0	15.8	-5.6	-1.8	14.1	-7.3
$TS_{C2aW-C3aW}$	12.6	29.4	8.0	10.8	27.4	6.0
C3aW	-11.8	3.8	-17.6	-12.8	3.0	-18.4
$TS_{C3aW-C4aW}$	-8.0	7.4	-13.9	-8.3	6.5	-14.7
C4aW	-12.9	2.5	-18.8	-14.1	1.3	-20.1
$TS_{C4aW-T4bW}$	-0.8	11.7	-9.6	4.9	17.5	-3.8
T4bW	-5.3	-1.4	-7.6	1.3	4.4	-1.8
$TS_{T4bW-T4cWN}$	3.7	11.6	0.2	9.8	17.2	5.8
$T4cW_N$	-8.5	-0.3	-11.7	-5.1	2.7	-8.7
$T4cW_{Rp}$	-8.1	-0.5	-11.9	-4.5	2.7	-8.7
$TS_{T4cWRp-T4dWRp}$	5.5	14.1	2.6	8.5	17.3	5.9
$T4dW_{Rp}$	4.0	11.0	-0.4	7.3	14.1	2.7
$TS_{T4dWRp-T4dNWRp}$	8.2	22.4	-3.4	11.2	26.8	5.8
$T4dNW_{Rp}$	0.4	15.6	-10.3	1.8	17.2	-3.7
$TS_{T4dNWRp-CW-C1aP.}$	5.6	20.4	-5.4	7.8	22.4	1.6
CW-C1aP.	3.1	16.6	-9.1	4.7	18.3	-2.6
$T4dNW_{Rp}L$	-1.0	22.9	-18.1	-0.3	22.4	-13.5
$TS_{T4dNWRp-C1aWP.}$	4.2	25.0	-15.9	7.4	30.0	-6.0
C1aWP.	-15.7	7.6	-33.3	-22.0	1.2	-34.8
CW-C1aW	7.6	10.8	6.5	13.6	16.1	11.7
$TS_{CW-C1aW-CW-C2aW}$	12.4	23.3	7.4	18.0	28.4	12.5
CW-C2aW	6.5	17.7	1.7	11.8	22.5	6.5
$TS_{CW-C2aW-CW-C3aW}$	12.2	24.0	8.1	17.9	30.3	14.3
CW-C3aW	-7.4	4.3	-11.7	-2.1	9.2	-6.8
$TS_{CW-C3aW-T4b2W}$	-7.5	3.1	-12.9	-0.8	10.3	-5.6
T4b2W	-9.8	0.2	-15.8	-4.4	5.8	-10.2
$TS_{T4b2W-T4c2WN}$	-0.8	14.1	-7.1	4.1	18.9	-2.2

T4c2W$_N$	-12.6	1.9	-19.3	-10.3	4.3	-16.9
T4cW$_{Rp}$W$_R$	-14.6	-1.7	-22.8	-11.7	1.1	-20.0
TS$_{T4cWRpWR-T4dWRpWR}$	1.0	16.0	-5.1	3.0	17.6	-3.5
T4dW$_{Rp}$W$_R$	0.4	13.5	-7.6	3.0	15.8	-5.3
T4d2W$_{Rp}$	-0.4	13.7	-7.4	2.0	15.7	-5.4
TS$_{T4d2WRp-T4dN2WRp}$	1.2	22.2	-13.4	2.3	23.7	-6.9
T4dN2W$_{Rp}$	-4.2	19.2	-16.4	-3.5	19.9	-10.7
TS$_{T4dN2WRp-CW-C1aWP.}$	-3.0	18.0	-17.4	0.6	22.0	-8.6
CW-C1aWP.	-5.7	16.2	-19.4	-6.2	17.1	-13.5
Structures in the supporting information:						
Complexes with water:						
CW-C1a	15.7	10.8	16.2	23.6	18.6	24.0
TS$_{CW-C1a-CW-C2a}$	17.0	20.7	14.5	23.3	26.5	20.3
CW-C2a	11.0	15.8	9.6	16.8	21.1	14.9
TS$_{CW-C2a-CW-C3a}$	16.5	20.4	14.3	23.8	27.4	21.2
CW-C3a	-4.4	0.9	-5.4	1.7	5.6	-0.7
TS$_{CW-C3a-T4bW}$	-1.3	2.9	-3.4	6.1	9.5	3.2
TS$_{T4cWN-T4dNWN}$	9.6	25.5	-0.4	11.1	26.3	5.4
T4dNW$_N$	5.3	19.8	-6.1	5.1	21.1	0.1
TS$_{T4dNWN-CW-C1aP.'}$	7.1	20.2	-5.7	10.7	24.5	3.6
CW-C1aP.'	3.2	17.2	-8.6	4.8	19.1	-1.8
C1a2W	-11.5	0.9	-18.6	-13.1	0.3	-19.2
TS$_{C1a2W-C2a2W}$	-5.6	15.6	-15.5	-8.2	13.0	-18.0
C2a2W	-6.4	14.6	-16.5	-8.7	12.9	-18.2
TS$_{C2a2W-C3a2W}$	5.6	27.6	-3.5	3.9	26.5	-4.6
C3a2W	-18.1	3.7	-27.4	-19.8	1.7	-29.4
TS$_{C3a2W-C4a2W}$	-10.8	11.1	-20.0	-12.5	9.1	-22.0
C4a2W	-17.6	4.6	-26.6	-20.0	2.3	-28.8
TS$_{C4a2W-T4b2W}$	-5.7	13.1	-18.0	-1.6	18.6	-12.5
TS$_{T4c2WN-T4dN2WN}$	3.8	26.3	-9.4	4.7	27.6	-3.1
T4dN2W$_N$	0.5	22.2	-13.4	-0.4	22.5	-8.3
TS$_{T4dN2WN-CW-C1aWP'}$	1.1	22.6	-13.1	3.1	22.3	-8.4
CW-C1aWP.'	-6.9	14.2	-21.3	-0.8	18.3	-12.3
T4cW$_N$W$_{Rp}$	-15.0	-1.3	-22.4	-12.1	1.1	-20.0
TS$_{T4cWNWRp-T4dWNWRp}$	1.6	16.9	-4.2	3.4	18.1	-3.1

T4dW$_N$W$_{Rp}$	1.8	16.1	-5.0	4.1	18.3	-2.8
TS$_{T4dWNWRp-T4dNWNWRp}$	5.3	26.6	-9.0	3.7	26.8	-3.9
T4dNW$_N$W$_{Rp}$	-0.7	21.2	-14.5	-1.1	20.7	-10.0
TS$_{T4dNWNWRp-CW-C1aWP.}$	-0.4	20.9	-14.7	2.7	22.8	-7.8
TS$_{T4dWRpWR-T4dNWRpWR}$	4.3	25.2	-10.4	3.7	26.8	-3.9
T4dNW$_{Rp}$W$_R$	-4.8	16.4	-19.2	-1.1	20.7	-10.0
TS$_{T4dNWRpWR-CW-C1aWP.}$	-3.0	18.0	-17.4	2.7	22.8	-7.8
T4c2W$_{Rp}$	-14.6	-1.9	-22.9	-11.8	0.9	-20.1
TS$_{T4c2WRp-T4d2WRp}$	6.9	22.7	1.5	8.4	23.8	2.6
T4d2W$_{Rp}$	-0.4	13.7	-7.4	2.0	15.7	-5.4
Complexes with methanol:						
C1aM	-6.7	1.1	-11.4	-8.5	-0.4	-12.9
TS$_{C1aM-C2aM}$	0.1	14.7	-9.5	-2.1	12.2	-11.9
C2aM	0.6	16.1	-8.0	-2.1	13.8	-10.3
TS$_{C2aM-C3aM}$	8.2	24.2	0.2	8.8	25.4	1.3
C3aM	-11.9	2.7	-21.3	-12.7	1.2	-22.8
TS$_{C3aM-C4aM}$	-8.6	6.6	-17.4	-9.2	6.2	-17.8
C4aM	-12.4	2.6	-21.5	-13.4	0.7	-23.4
TS$_{C4aM-C5aM}$	-9.2	6.5	-17.6	-9.3	5.8	-18.2
C5aM	-14.1	1.3	-22.8	-15.6	-0.4	-24.4
TS$_{C5aM-T4bM}$	-1.5	12.4	-11.6	3.4	16.5	-7.5
T4bM	-6.1	-1.8	-10.7	0.3	5.3	-3.6
CM-C1a	15.7	11.8	14.4	23.7	19.4	22.0
TS$_{CM-C1a-CM-C2a}$	15.8	21.5	12.6	21.9	26.6	17.6
CM-C2a	9.6	15.8	6.9	15.0	20.6	11.6
TS$_{CM-C2a-CM-C3a}$	15.8	21.2	12.3	22.6	28.1	19.1
CM-C3a	-5.9	1.0	-8.0	-0.2	6.6	-2.4
TS$_{CM-C3a-T4bM}$	-2.0	3.3	-5.7	5.4	10.3	1.3
TS$_{T4bM-T4cMN}$	2.7	10.7	-3.5	8.6	15.7	1.5
T4cM$_N$	-9.3	-0.5	-14.7	-6.5	1.6	-12.6
T4cM$_{Rp}$	-9.3	-1.2	-15.3	-6.0	1.5	-12.6
TS$_{T4cMRp-T4dMRp}$	2.7	12.3	-1.9	4.9	14.3	0.1
T4dM$_{Rp}$	2.2	10.8	-3.3	4.9	12.4	-1.7
TS$_{T4dMRp-T4dNMRp}$	7.0	22.8	-5.8	9.2	25.0	1.3
T4dNM$_{Rp}$	-0.3	16.8	-11.9	0.3	16.6	-7.1

$TS_{T4dNMRp\text{-}CM\text{-}C1aP.}$	4.3	17.4	-11.2	7.0	21.1	-2.6
CM-C1aP.	4.2	18.4	-10.1	7.1	22.5	-1.1
C1a2M	-13.2	1.2	-23.7	-15.1	-0.5	-25.5
$TS_{C1a2M\text{-}C2a2M}$	-6.5	15.2	-21.4	-9.4	12.7	-23.8
C2a2M	-8.6	14.0	-22.6	-11.4	11.7	-24.9
$TS_{C2a2M\text{-}C3a2M}$	1.3	24.3	-12.2	-0.4	23.3	-13.3
C3a2M	-21.4	1.9	-34.7	-23.7	0.2	-36.4
$TS_{C3a2M\text{-}C4a2M}$	-15.8	7.0	-29.4	-16.6	6.9	-29.5
C4a2M	-20.4	2.3	-34.2	-22.6	0.3	-36.2
$TS_{C4a2M\text{-}T4b2M}$	-8.3	11.4	-25.1	-3.9	16.2	-20.3
T4b2M	-13.0	-1.6	-23.0	-7.1	3.5	-17.9
CM-C1aM	5.8	11.4	1.5	11.8	17.5	7.6
$TS_{CM\text{-}C1aM\text{-}CM\text{-}C2aM}$	10.6	24.4	3.0	21.9	26.6	17.6
CM-C2aM	4.4	18.9	-2.5	15.0	20.6	11.6
$TS_{CM\text{-}C2aM\text{-}CM\text{-}C3aM}$	10.8	25.5	4.1	22.6	28.1	19.1
CM-C3aM	-9.4	5.4	-16.1	-0.2	6.6	-2.4
$TS_{CM\text{-}C3aM\text{-}T4b2M}$	-9.1	4.1	-17.3	5.4	10.3	1.3
$TS_{T4b2M\text{-}T4c2MN}$	-4.1	11.3	-15.3	1.2	16.5	-10.1
$T4c2M_N$	-15.7	0.2	-26.5	-13.5	2.3	-24.3
$T4cM_{Rp}M_R$	-16.3	-1.3	-27.9	-13.9	1.4	-25.2
$TS_{T4cMRpMR\text{-}T4dMRpMR}$	-2.0	14.6	-12.0	-0.9	15.3	-11.3
$T4dM_{Rp}M_R$	-2.2	11.5	-15.1	0.0	14.6	-11.9
$T4d2M_{Rp}$	-3.5	11.9	-14.7	-1.8	13.1	-13.4
$TS_{T4d2MRp\text{-}T4dN2MRp}$	-2.0	20.4	-20.7	-1.2	21.5	-14.7
$T4dN2M_{Rp}$	-7.5	15.9	-25.2	-7.2	16.8	-19.4
$TS_{T4dN2MRp\text{-}CM\text{-}C1aMP.}$	-2.4	17.5	-23.6	-0.1	21.3	-14.8
CM-C1aMP.	-4.9	17.5	-23.5	-4.2	17.9	-18.1
Complexes with dimethylamine:						
CA-C1a	13.4	12.1	13.4	18.7	16.7	18.0
$TS_{CA\text{-}C1a\text{-}CA\text{-}C2a}$	14.9	22.2	12.0	18.6	25.7	15.4
CA-C2a	12.4	20.7	10.4	15.8	23.3	13.0
$TS_{CA\text{-}C2a\text{-}CA\text{-}C3a}$	21.5	29.2	18.9	27.8	36.0	25.7
CA-C3a	-3.3	5.3	-5.0	0.1	8.4	-1.9
$TS_{CA\text{-}C3a\text{-}T4bA}$	2.2	8.5	-1.7	9.2	16.2	5.9
T4bA	-3.2	1.0	-9.2	3.3	7.4	-2.8

$TS_{T4bA-T4cAN}$	6.8	15.4	0.0	12.7	21.3	5.9
$T4cA_N$	-5.2	4.2	-11.2	-2.1	7.4	-8.0
$T4cA_{Rp}$	-6.3	1.1	-14.3	-2.8	5.5	-9.9
$TS_{T4cARp-T4dARp}$	4.5	15.9	0.4	6.3	17.4	1.9
$T4dA_{Rp}$	2.4	12.5	-2.9	4.1	14.0	-1.5
$TS_{T4dARp-CA-C1a+P.}$	9.5	19.3	4.0	12.2	19.5	4.1
CA-C1a+P.	5.6	13.8	0.4	6.4	14.0	0.6
CA-C1aA	9.8	17.0	4.6	13.8	20.3	7.9
$TS_{CA-C1aA-CA-C2aA}$	12.8	28.1	4.1	15.5	30.7	6.7
CA-C2aA	10.9	27.0	2.9	13.4	29.7	5.7
$TS_{CA-C2aA-CA-C3aA}$	16.6	30.2	6.2	20.5	34.5	10.5
CA-C3aA	-2.8	12.8	-11.2	-1.3	13.4	-10.6
$TS_{CA-C3aA-T4b2A}$	-1.5	10.3	-13.7	4.5	17.2	-6.8
T4b2A	-5.5	5.0	-18.9	0.0	11.3	-12.7
$TS_{T4b2A-T4c2AN}$	3.2	18.9	-10.3	7.4	22.6	-6.6
$T4c2A_N$	-8.9	6.7	-22.4	-5.0	11.1	-18.1
$T4c2A_{Rp}$	-10.2	5.8	-23.3	-7.5	7.1	-22.1
$TS_{T4c2ARp-T4dARpAR}$	-0.1	16.0	-13.2	1.2	19.1	-10.1
$T4dA_{Rp}A_R$	-2.6	13.6	-15.6	-1.6	15.2	-13.9
$T4dA_{Rp}A_N$	0.9	18.8	-10.5	1.4	18.9	-10.3
$TS_{T4dARpAN-CA-C1aA+P.}$	4.2	21.8	-7.4	8.1	26.3	-2.9
CA-C1aA+P.	2.1	18.7	-8.5	1.4	17.6	-9.6

* The energy/free energy is relative to **C1a** and the individual small molecules.

4. Label of structures and naming of N, R and Rp

The labels of the structures basically follow our previous study on $(PMe_3)_4RuH_2$ and $(dmpe)_2RuH_2$.[6] Taking **C1aW** as the example, it represents $(PMe_3)_4RuH_2$ (**C1a**) with one solvent water (**W**). Correspondingly the **M** and **A** is used for methanol and dimethylamine respectively. For the water coordinated complex, the prefix of **CW** is added to represent substituting a PMe_3 by the coordinated water. For instance, **CW-C1a** represents $(PMe_3)_3RuH_2(H_2O)$.

In the metathesis and $HCOOH{\cdot}NMe_3$ elimination process, the influence of the additive molecules becomes more complicated. Besides the number of additive molecules, the position of them is also important. To show the position of additive molecules, as shown in Scheme S1, we will take three typical water positions with the notation of **N, R** and **Rp**. **N** represents the non-reaction binding site in the metathesis reaction; **R** represents the reaction site in the metathesis reaction; **Rp** represents the metathesis reaction involving a proton transfer with water or other additive at **R** position. They are used as a subscript followed by the **W** (water), **M** (methanol) or **A**(dimethylamine) in the label, as the examples shown in Scheme S1.

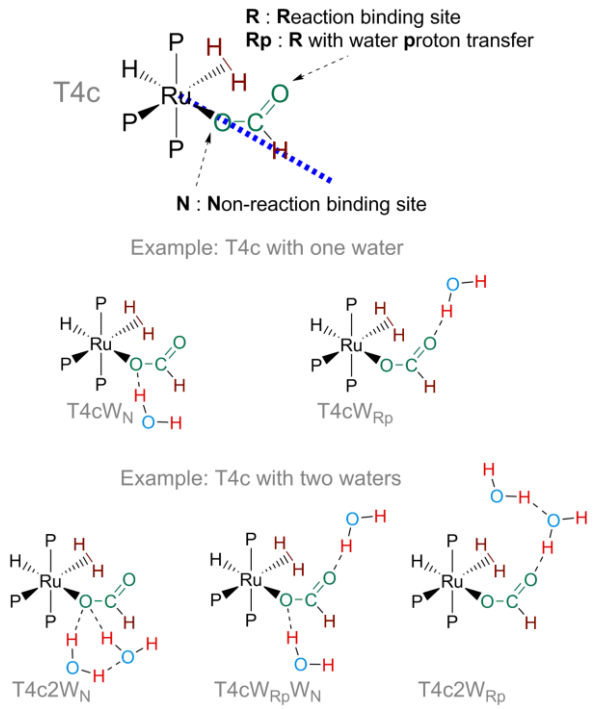

Scheme S1: Different binding sites of the additive molecules with the notation of **N**, **R**, **Rp**.

5. Supplementary Reactions

5.1 Supplementary Reaction of one H_2O

5.1.1 CO_2 insertion & intramolecular ligand substitution of $(PMe_3)_3RuH_2(H_2O)$

As shown in Figure S1, CO_2 can direct insert into $(PMe_3)_3RuH_2(H_2O)$ (**CW-C1a**), and the coordinated water can help with this insertion with a hydrogen bond, which has been studied by Munshi *et. al.* previously.[7] In their study the CO_2 insertion barrier of $(PMe_3)_3RuH_2(H_2O)$ calculated by B3LYP is 6.8 kcal/mol, while the intramolecular substitution barrier of the coordinated water is 3.6 kcal/mol. This has a good accordance with our barriers here with 5.5 kcal/mol for CO_2 insertion and 3.1 kcal/mol for substitution of coordinated water respectively.

The coordinated water will form a strong hydrogen bond of 1.58Å with the $HCOO^-$ in **CW-C2a**, which helps the rotation of the $HCOO^-$ ion as a rotation shaft. Comparing to CO_2 insertion without coordinated water in Figure 3, this hydrogen bond leads to the smaller CO_2 insertion barrier. In addition, as the coordination energy of water is considerably lower than that of PMe_3, comparing to **C5aW** in Figure 3, the **CW-C3a** can more easily go through the intramolecular ligand substitution both energetically and dynamically.

Besides water coordinate complex($(PMe_3)_3(H_2O)RuH_2$), the reaction pathway involving CO_2 coordination complex($(PMe_3)_3(CO_2)RuH_2$) is also considered, which relative energy and structure is already involved in Fig. 2 of our previous study[6]. However, CO_2 is not a good ligand with the coordination energy of only 2.8 kcal/mol. With the coordination energy of 6.7 kcal/mol, the water is a better ligand. This means the ligand substitution reaction from $(PMe_3)_3(H_2O)RuH_2$ to $(PMe_3)_3(CO_2)RuH_2$ could not take place. In addition, due to the aggregation of the waters around the hydrophilic product ($HCOOH{\cdot}NMe_3$), in the product disassociation process in Fig. 5, the water will soon coordinate on the active site generating $(PMe_3)_3(H_2O)RuH_2$ rather than $(PMe_3)_3(CO_2)RuH_2$. Hence the reaction pathway involving $(PMe_3)_3(CO_2)RuH_2$ could be ruled out.

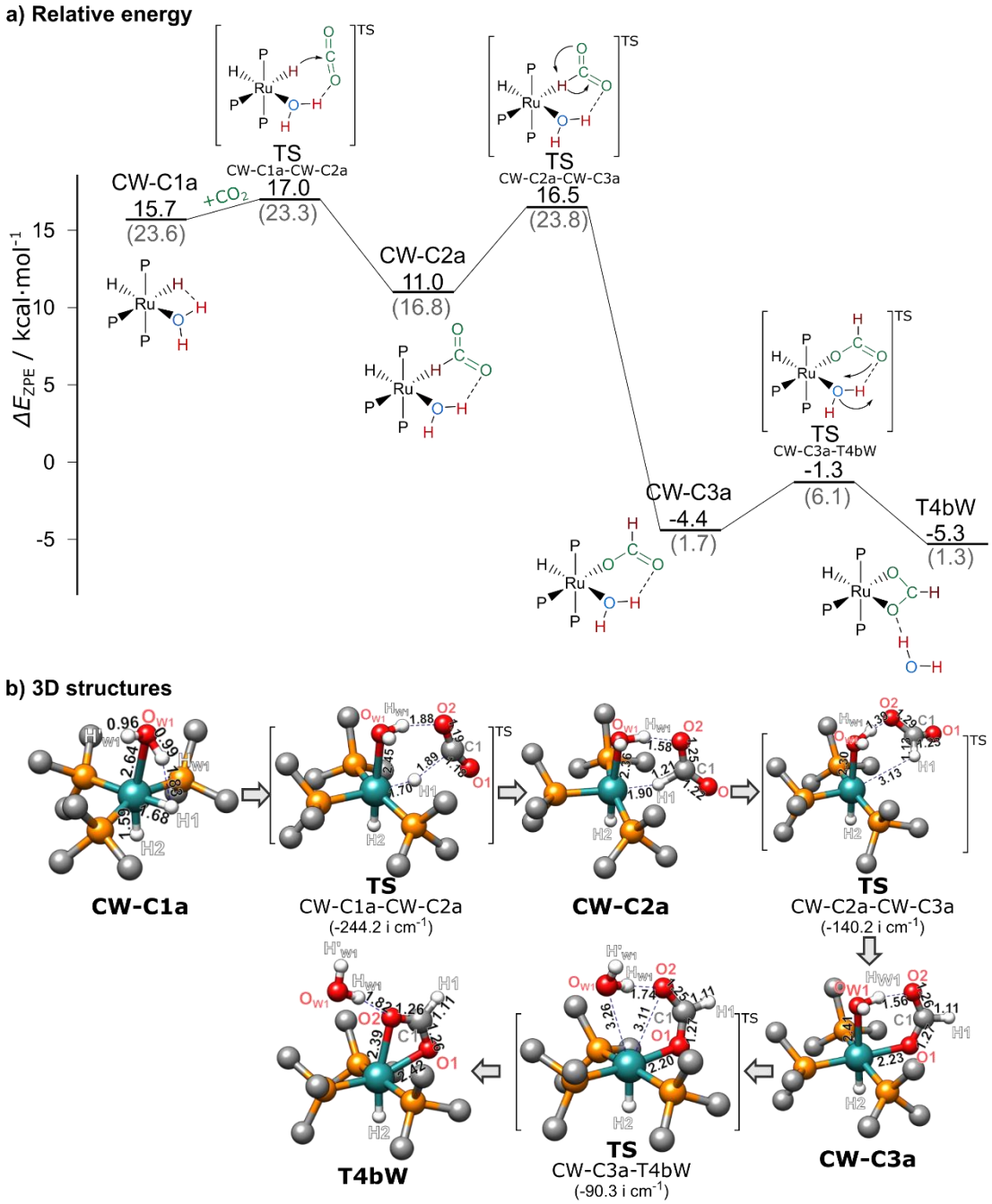

Figure S5: The reaction path for CO_2 insertion into $(PMe_3)_3RuH_2(H_2O)$, leading to the formation of η^2-OOCH complex. a) Relative Energy for the intermediate and transition structures in kcal/mol, with B3LYP results indicated by black lines and black numbers and PBE0 results in gray parenthesis; b) 3D structures, with the hydrogen atoms on the methyl groups omitted.

5.1.2 Comparison between W_N & W_{Rp} pathway in the metathesis and $HCOOH{\cdot}NMe_3$ elimination step.

As shown in Scheme 2, after the intramolecular ligand disassociation, the coordinated H_2O on $(PMe_3)_3RuH(H_2O)(OOCH)$ will be substituted by the uncoordinated O on $OOCH^-$ forming the η^2-OOCH complex with one solvent water. Hence the pathways of **CW-C1a** and **C1aW** become identical after the formation of the η^2-OOCH complex (**T4b**), and the following pathway is shown in Figure 4. However, the position of water is important in the metathesis and $HCOOH{\cdot}NMe_3$ elimination step. In the MD trajectories, the water molecules can change their binding sites from time to time. Although with the limit computational cost only one or two waters are considered in this study, we should still take all typical water binding sites into account and find out the most favorable pathway.

The favorable $\mathbf{W_{Rp}}$ pathway has been shown in Figure 4, and our constrain calculation shows the water at R binding site will go through the proton transfer process in the metathesis step. Here the alternative $\mathbf{W_N}$ pathway is also presented, as shown in Figure S6. Because of the binding water at N site, the structure of $\mathbf{T4dW_N}$ is not stable and the local minimal cannot be obtained, but we can still get the transition state by inserting NMe_3. By comparing the relative energies of transition states, it is obvious that the $\mathbf{W_N}$ pathway ($\mathbf{TS_{T4cWN\text{-}T4dNWN}}$, 9.6 kcal/mol) in Figure S5 is less favorable than the $\mathbf{W_{Rp}}$ pathway ($\mathbf{TS_{T4dWRp\text{-}T4dNWRp}}$, 8.6 kcal/mol) in Figure 4.

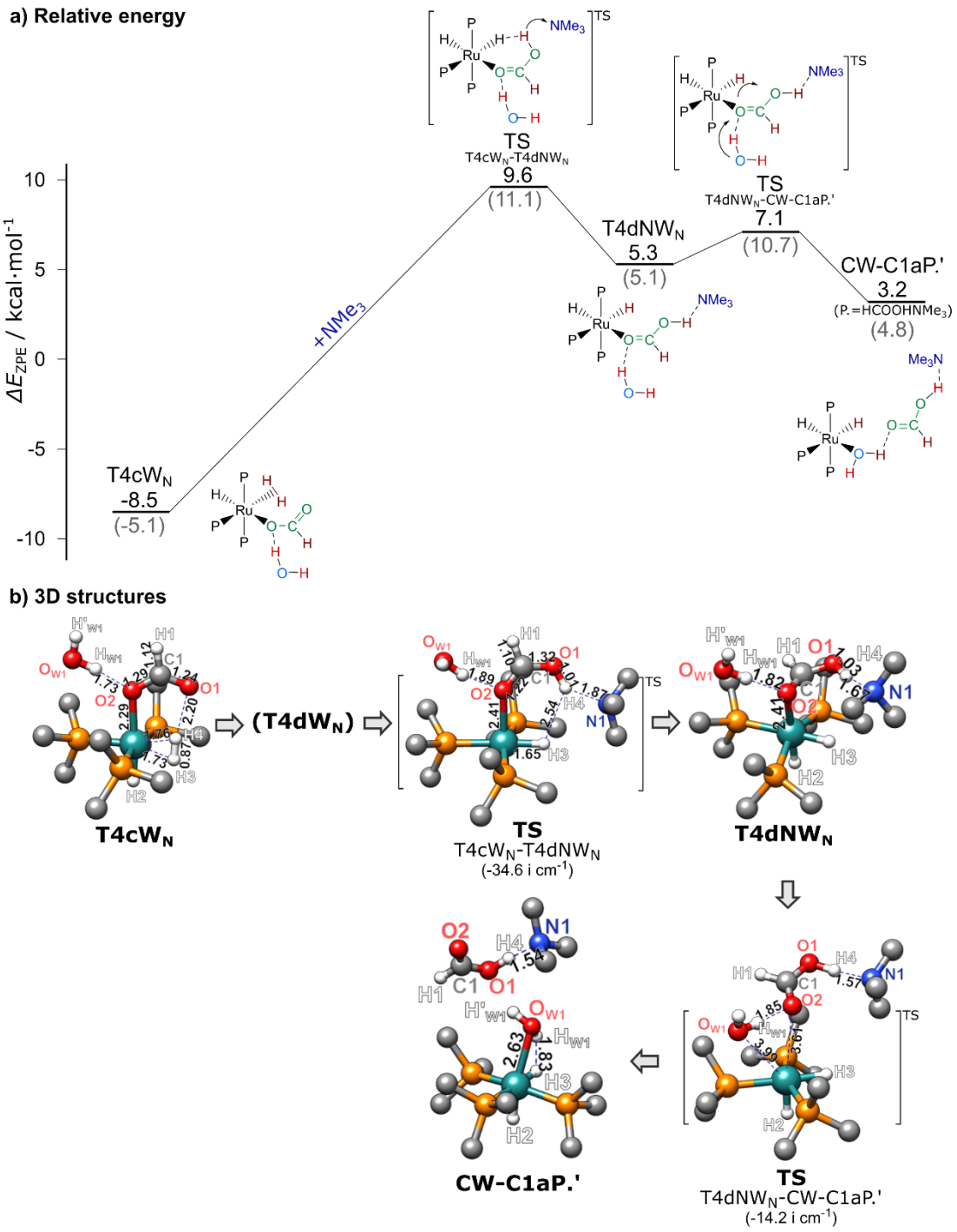

Figure S6: Metathesis and the elimination of HCOOH·NMe$_3$, the **W$_N$** pathway. a) Relative Energy for the intermediate and transition structures in kcal/mol, with B3LYP results indicated by black lines and black numbers and PBE0 results in gray parenthesis; b) 3D structures, with the hydrogen atoms on the methyl groups omitted.

5.2 Supplementary Reaction of two H_2O

5.2.1 CO_2 insertion & intramolecular ligand substitution of $(PMe_3)_4RuH_2 \cdot 2H_2O$

As shown in Figure S7, when the $(PMe_3)_4RuH_2$ is solvated by two H_2O, the CO_2 insertion and intramolecular ligand disassociation processes are similar to the case with one solvent H_2O. Both the barriers change little comparing to the case in Figure 3, although each corresponding relative energy is lowered by the binding of the second solvent H_2O.

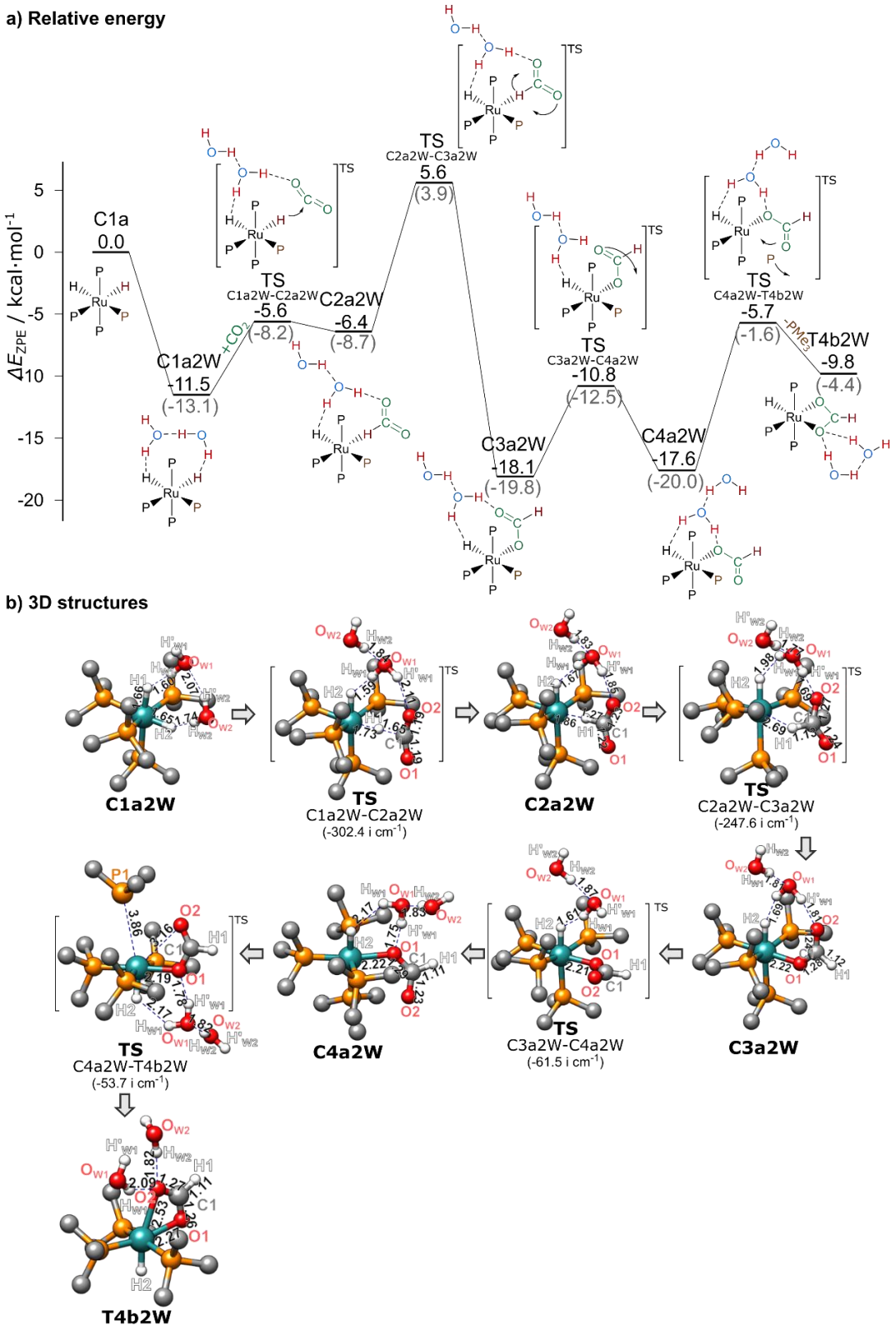

Figure S7. The reaction path for the direct CO_2 insertion into $(PMe_3)_4RuH_2$, leading to the formation of η^2-OOCH complex, with two solvent H_2O. a) Relative Energy for the intermediate and transition structures in kcal/mol, with B3LYP results indicated by black lines and black numbers and PBE0 results in gray parenthesis; b) 3D structures, with the hydrogen atoms on the methyl groups omitted.

5.2.2 Comparison among $2W_N$, W_NW_{Rp}, W_RW_{Rp} & $2W_{Rp}$ pathways in the metathesis and $HCOOH{\cdot}NMe_3$ elimination step.

When two solvent H_2O are considered in the metathesis and $HCOOH{\cdot}NMe_3$ elimination step, things are more complicated comparing to the case of one solvent water. In the Figure 9, only the favorable pathway is shown. Actually, all the four typical pathways ($\mathbf{2W_N}$, $\mathbf{W_NW_{Rp}}$, $\mathbf{W_RW_{Rp}}$ & $\mathbf{2W_{Rp}}$) have been calculated, as shown here in Figure S8-S11. By comparing the relative energies of the transition state of each reaction step, the favorable pathway can be rolled out. In this pathway, the metathesis follows the $\mathbf{W_RW_{Rp}}$ pathway in Figure S10, while the NMe_3 insertion and substitution of $HCOOHNMe_3$ follows $\mathbf{2W_{Rp}}$ pathway in Figure S11.

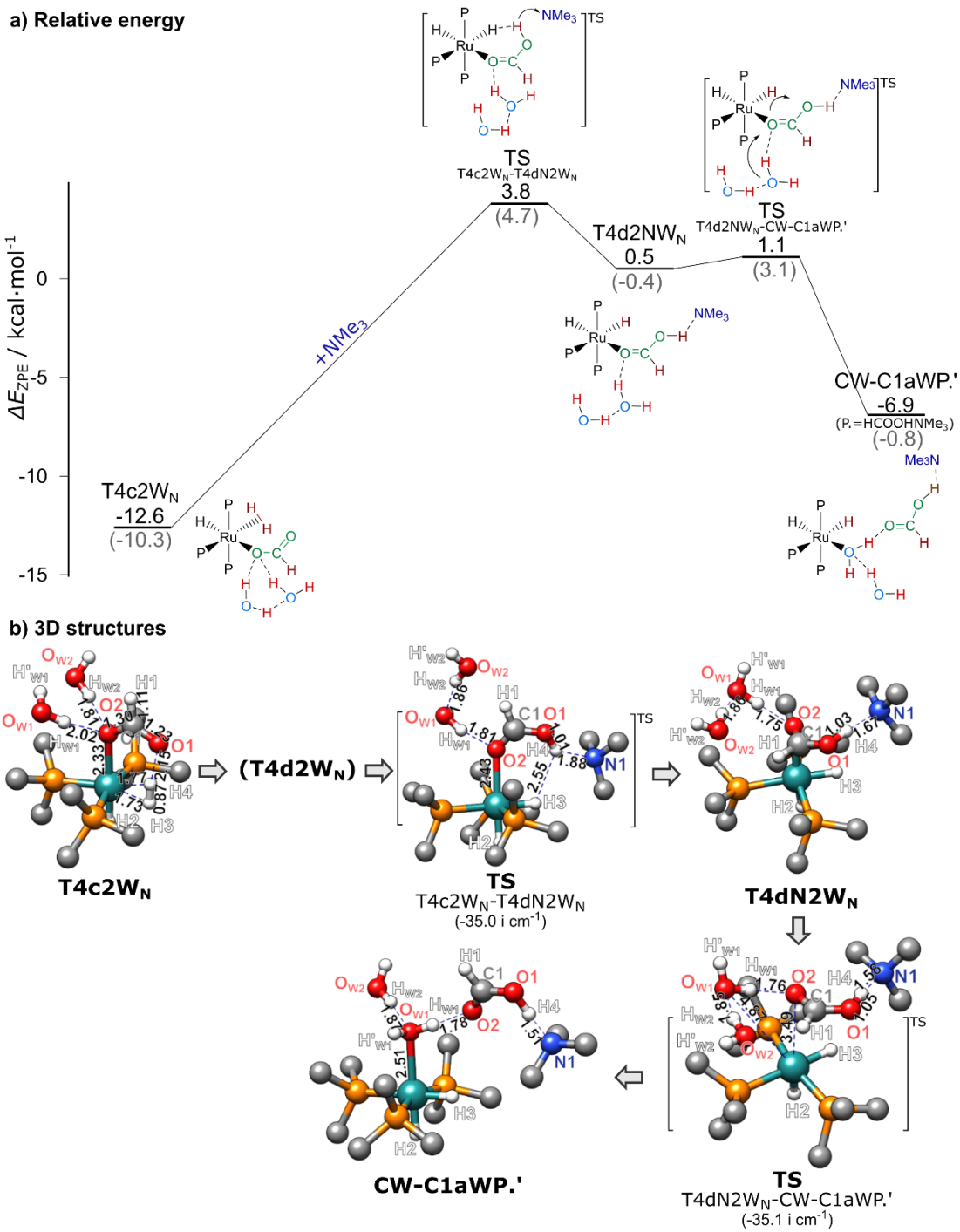

Figure S8. Metathesis and the elimination of HCOOH·NMe$_3$, the **2W$_N$** pathway. a) Relative Energy for the intermediate and transition structures in kcal/mol, with B3LYP results indicated by black lines and black numbers and PBE0 results in gray parenthesis; b) 3D structures, with the hydrogen atoms on the methyl groups omitted.

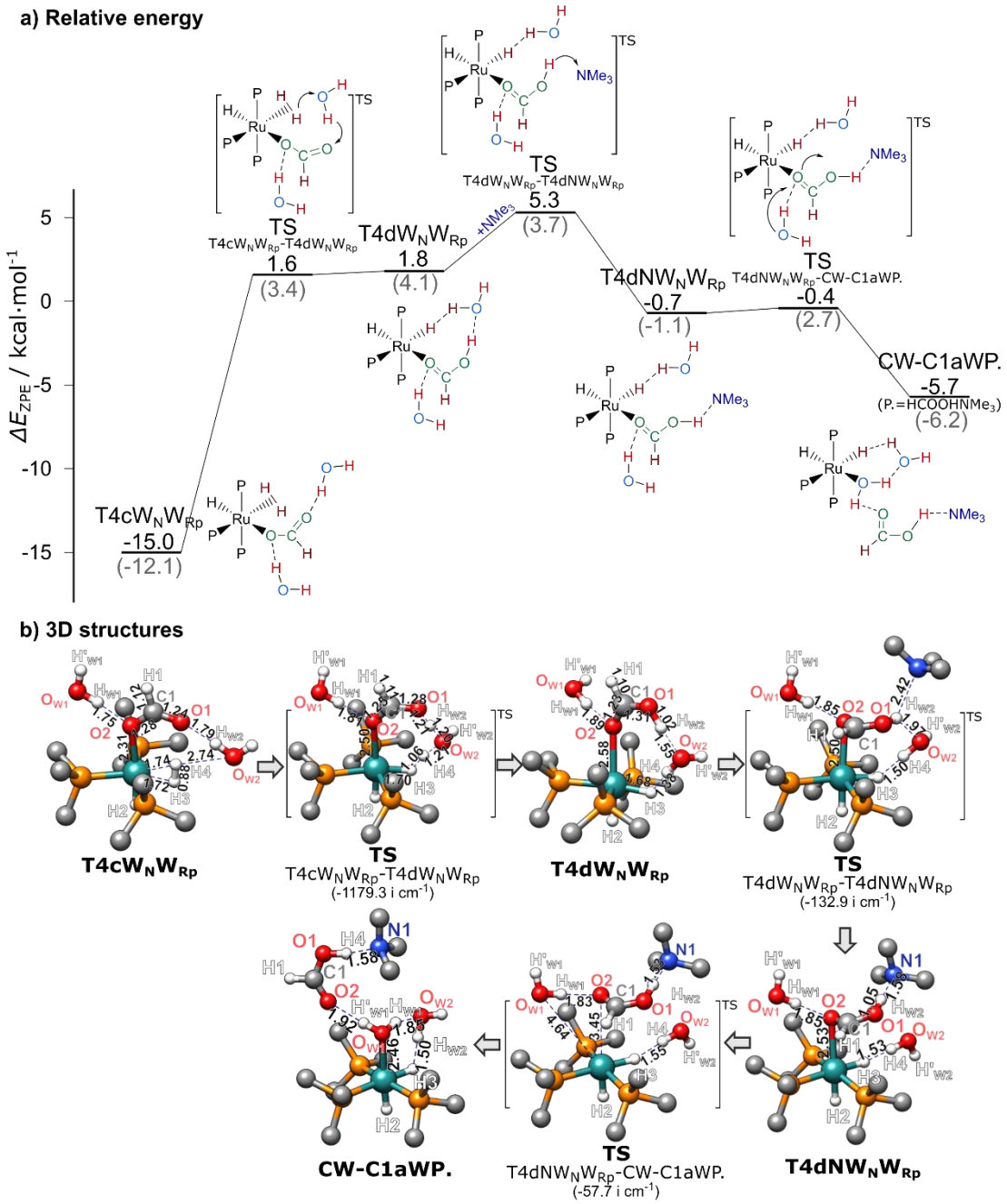

Figure S9. Metathesis and the elimination of HCOOH·NMe_3, the $\mathbf{W_NW_{Rp}}$ pathway. a) Relative Energy for the intermediate and transition structures in kcal/mol, with B3LYP results indicated by black lines and black numbers and PBE0 results in gray parenthesis; b) 3D structures, with the hydrogen atoms on the methyl groups omitted.

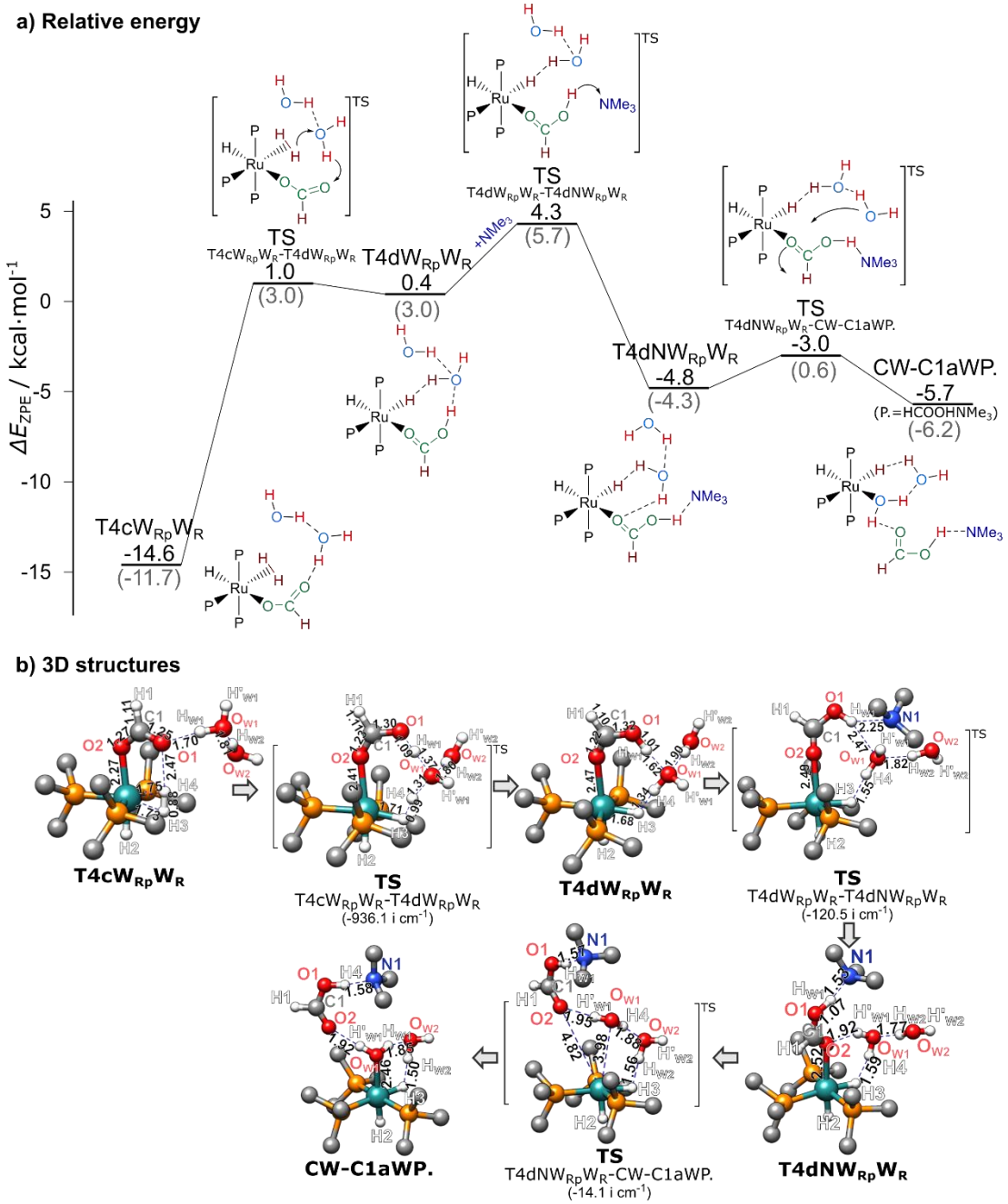

Figure S10. Metathesis and the elimination of HCOOH·NMe$_3$, the $\mathbf{W_RW_{Rp}}$ pathway. a) Relative Energy for the intermediate and transition structures in kcal/mol, with B3LYP results indicated by black lines and black numbers and PBE0 results in gray parenthesis; b) 3D structures, with the hydrogen atoms on the methyl groups omitted.

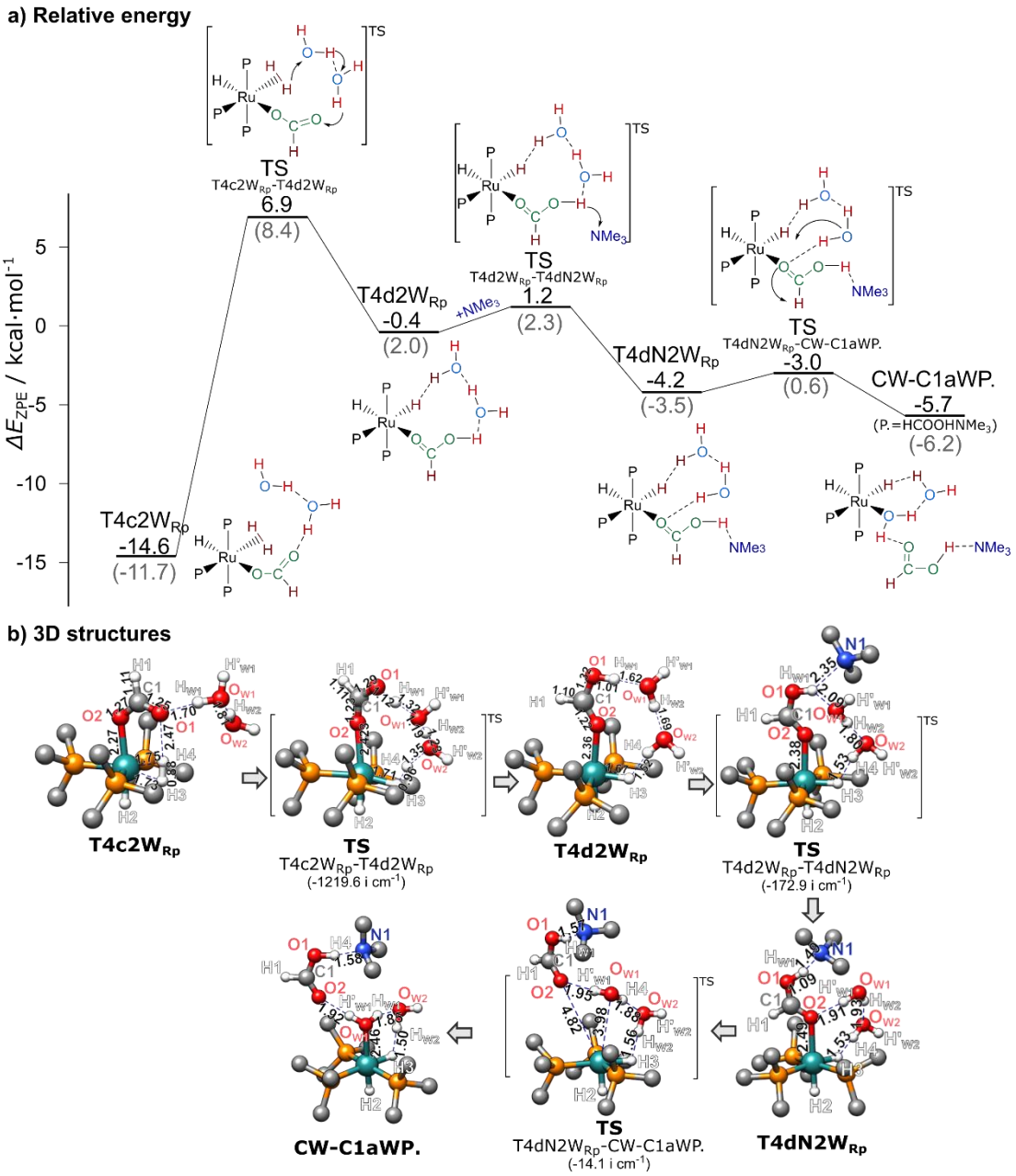

Figure S11. Metathesis and the elimination of HCOOH·NMe$_3$, the **2W$_{Rp}$** pathway. a) Relative Energy for the intermediate and transition structures in kcal/mol, with B3LYP results indicated by black lines and black numbers and PBE0 results in gray parenthesis; b) 3D structures, with the hydrogen atoms on the methyl groups omitted.

5.3 Reactions of one MeOH

5.3.1 CO_2 insertion & intramolecular ligand substitution of $(PMe_3)_4RuH_2$·MeOH

As shown in Figure S12, when the $(PMe_3)_4RuH_2$ is solvated by one MeOH, the CO_2 insertion and intramolecular ligand disassociation processes are similar to the case without any additive. Both the barriers change little, although each corresponding relative energy is lowered by the binding of the solvent MeOH. The CO_2 insertion barrier (14.9 kcal/mol) is slightly smaller than that in case of one solvent water (18.5 kcal/mol, in Figure 3), while the intramolecular ligand disassociation barrier is almost the same.

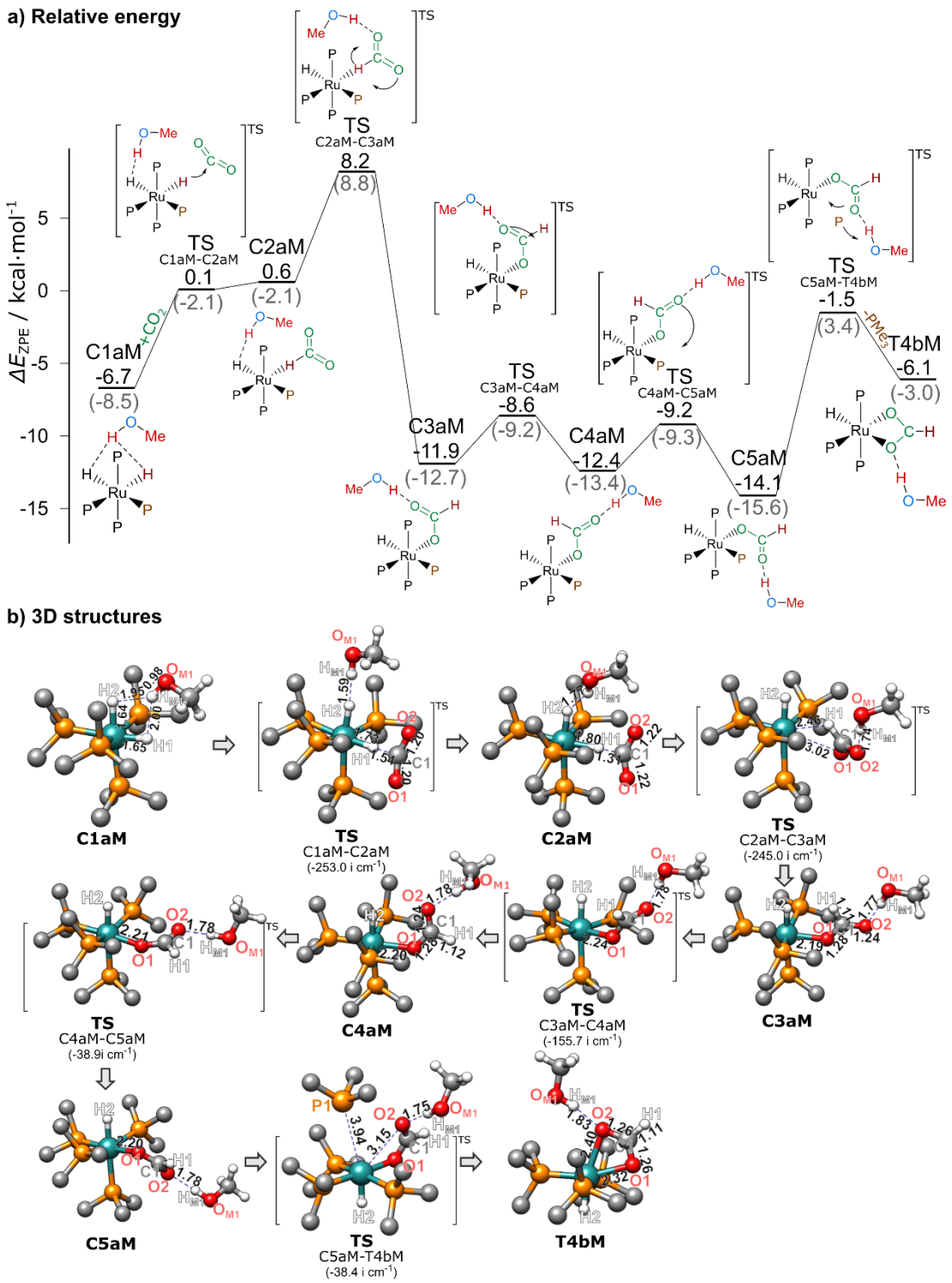

Figure S12. The reaction path for the direct CO_2 insertion into $(PMe_3)_4RuH_2$, leading to the formation of η^2-OOCH complex, with one MeOH solvent. a) Relative Energy for the intermediate and transition structures in kcal/mol, with B3LYP results indicated by black lines and black numbers and PBE0 results in gray parenthesis; b) 3D structures, with the hydrogen atoms on the methyl groups omitted.

5.3.2 CO_2 insertion & intramolecular ligand substitution of $(PMe_3)_3RuH_2(MeOH)$

As shown in Figure S13, CO_2 can also direct insert into $(PMe_3)_3RuH_2(MeOH)$ (**CM-C1a**), and the coordinated methanol can help with this insertion with a hydrogen bond, just like the case of one coordinated water. The barrier of CO_2 insertion into $(PMe_3)_3RuH_2(MeOH)$ is 6.2 kcal/mol, and that of intramolecular substitution of coordinated methanol is 3.9 kcal/mol. Both are slightly higher than that in case of $(PMe_3)_3RuH_2(H_2O)$.

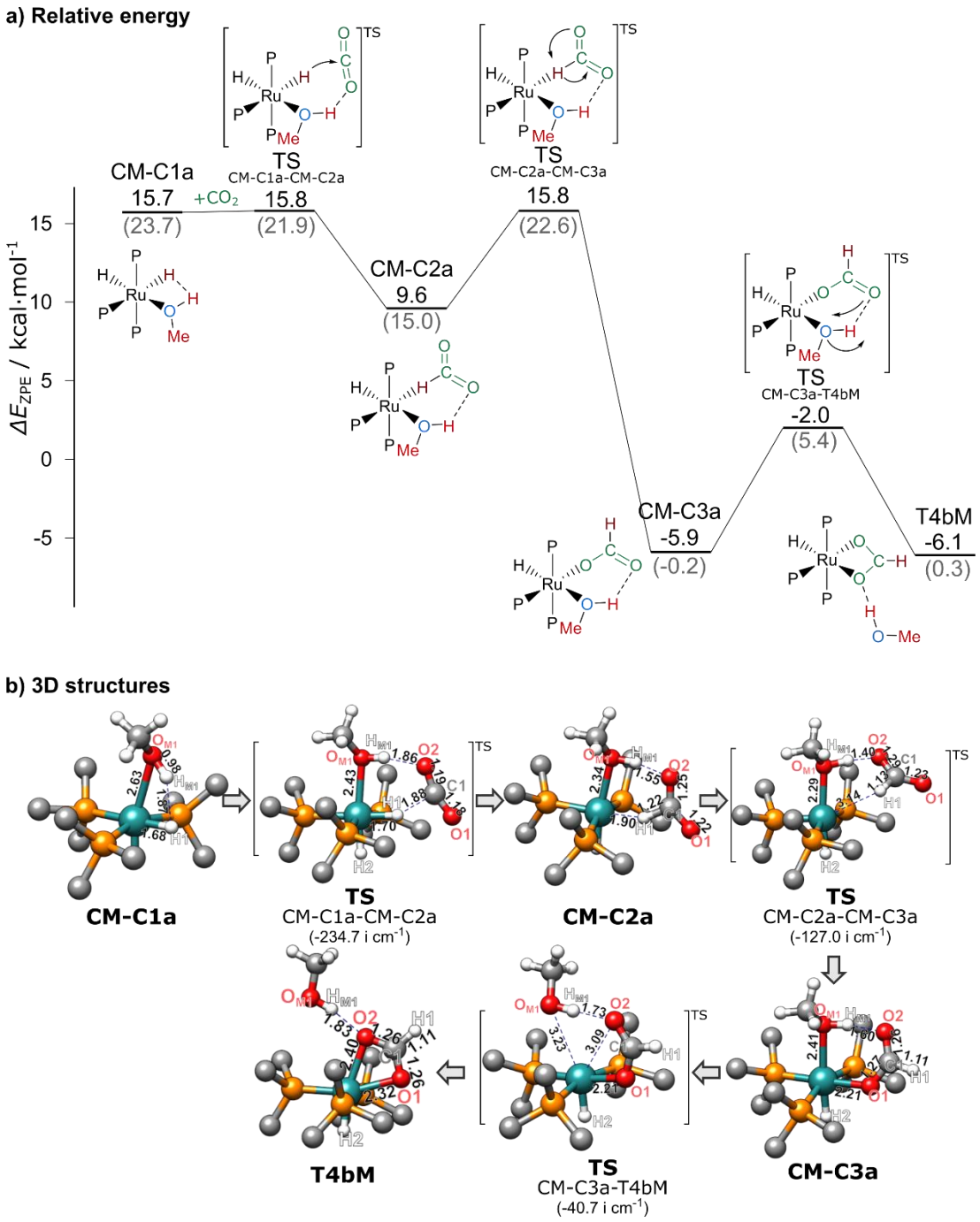

Figure S13. The reaction path for CO_2 insertion into $(PMe_3)_3RuH_2(MeOH)$, leading to the formation of η^2-OOCH complex. a) Relative Energy for the intermediate and transition structures in kcal/mol, with B3LYP results indicated by black lines and black numbers and PBE0 results in gray parenthesis; b) 3D structures, with the hydrogen atoms on the methyl groups omitted.

5.3.3 H_2 insertion, metathesis & $HCOOH{\cdot}NMe_3$ elimination with one solvent MeOH.

As shown in Figure S12, after the intramolecular ligand disassociation, the coordinated MeOH on $(PMe_3)_3RuH(MeOH)(OOCH)$ will be substituted by the uncoordinated O on $OOCH^-$ generating the η^2-OOCH complex with one solvent MeOH. Hence the pathway of **CM-C1a** and **C1aM** become identical after the formation of the η^2-OOCH complex (**T4b**), and the following pathway is shown in Figure S14. There also exists a competition on the $HCOOH{\cdot}NMe_3$ elimination step. As shown in Figure S14, the $HCOOH{\cdot}NMe_3$ can be substituted by one MeOH (with a barrier of 4.6 kcal/mol), which binds around the hydrophilic pocket with hydrogen bond, producing the $(PMe_3)_3RuH_2(MeOH)$ (**CM-C1a**). Alternatively, the $HCOOH{\cdot}NMe_3$ can be substituted by one PMe_3 solvated in the $scCO_2$ environment (with a barrier of 5.8 kcal/mol), regenerating $(PMe_3)_4RuH_2{\cdot}(MeOH)$ (**C1aM**), which is energetically more favorable. The barriers of these two processes are similar. However, as there exist abundant MeOH in the $scCO_2$ in the experiment[5], the aggregation of the MeOH additives will make the MeOH substitution dynamically more favorable. In addition, the formed $(PMe_3)_3RuH_2(MeOH)$ will soon react with the CO_2 in Figure S12, and go into the CO_2 hydrogenation reaction cycle, as the CO_2 insertion barrier is considerably small.

The position of the MeOH also have an important influence on the metathesis and $HCOOH{\cdot}NMe_3$ elimination step. Here in Figure S14, only the favorable $\mathbf{M_{Rc}}$ is presented. We also calculate the $\mathbf{M_N}$ pathway and its key relative energy of these transition state ($\mathbf{TS_{T4dMN\text{-}T4dNMN}}$) is slightly higher than that of $\mathbf{M_{Rc}}$ ($\mathbf{TS_{T4dMRc\text{-}T4dNMRc}}$) by 1.6 kcal/mol, which suggest the $\mathbf{M_{Rc}}$ is the more favorable pathway.

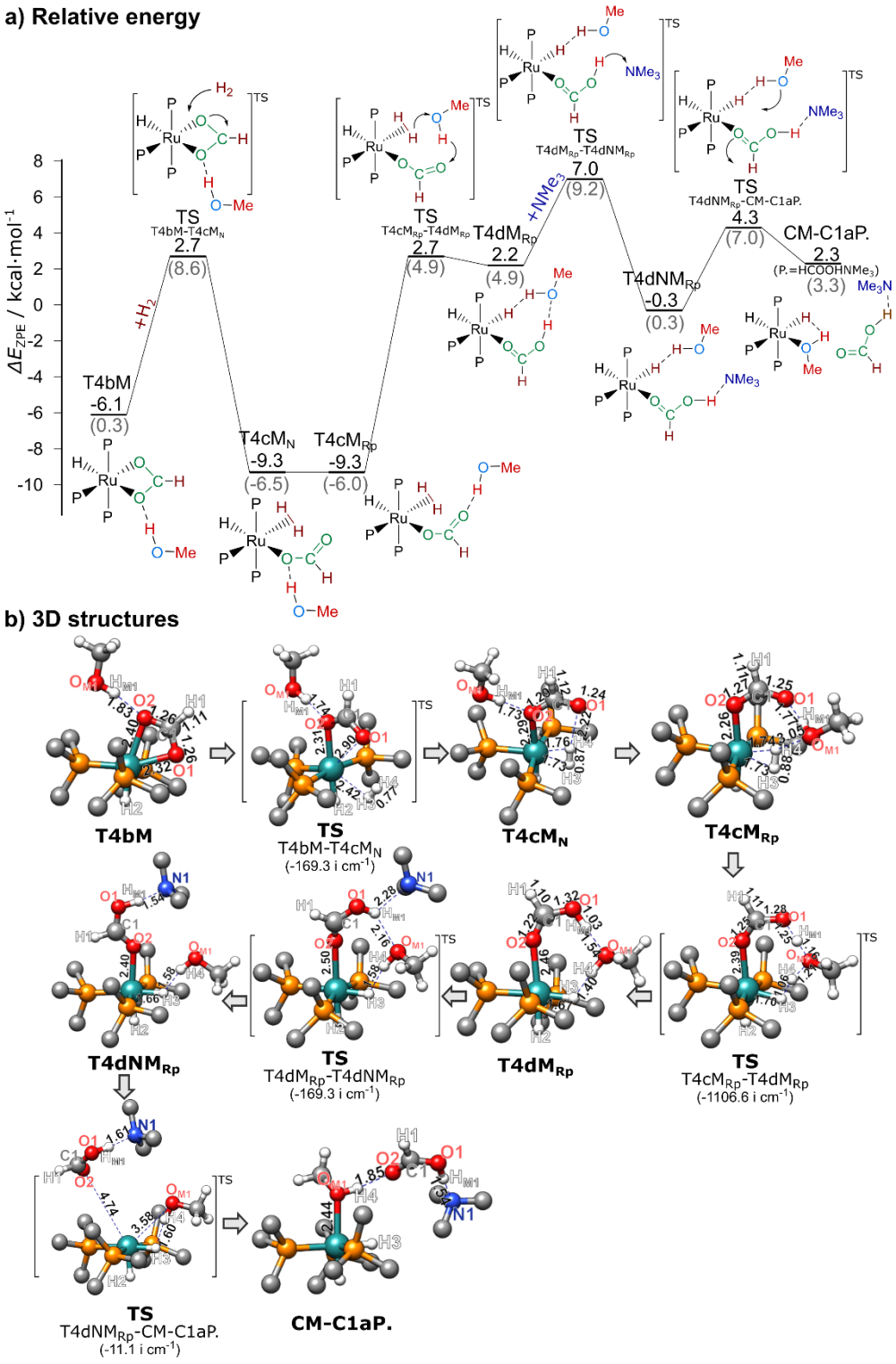

Figure S14. The reaction path for H_2 insertion into $(PMe_3)_3RuH(\eta^2\text{-}OOCH)$ followed by the metathesis and the elimination of $HCOOH{\cdot}NMe_3$, in presence of one MeOH. a) Relative Energy for the intermediate and transition structures in kcal/mol, with B3LYP results indicated by black lines and black numbers and PBE0 results in gray parenthesis; b) 3D structures, with the hydrogen atoms on the methyl groups omitted.

5.4 Reaction of 2 MeOH

5.4.1 *CO_2 insertion & intramolecular ligand substitution of $(PMe_3)_4RuH_2 \cdot 2MeOH$*

As shown in Figure S15, when the $(PMe_3)_4RuH_2$ is solvated by two MeOH, the CO_2 insertion and intramolecular ligand disassociation processes are similar to the case of one solvent MeOH. Although each corresponding relative energy is lowered by the binding of the second solvent MeOH, both the CO_2 insertion barrier and the intramolecular ligand disassociation barrier are almost the same.

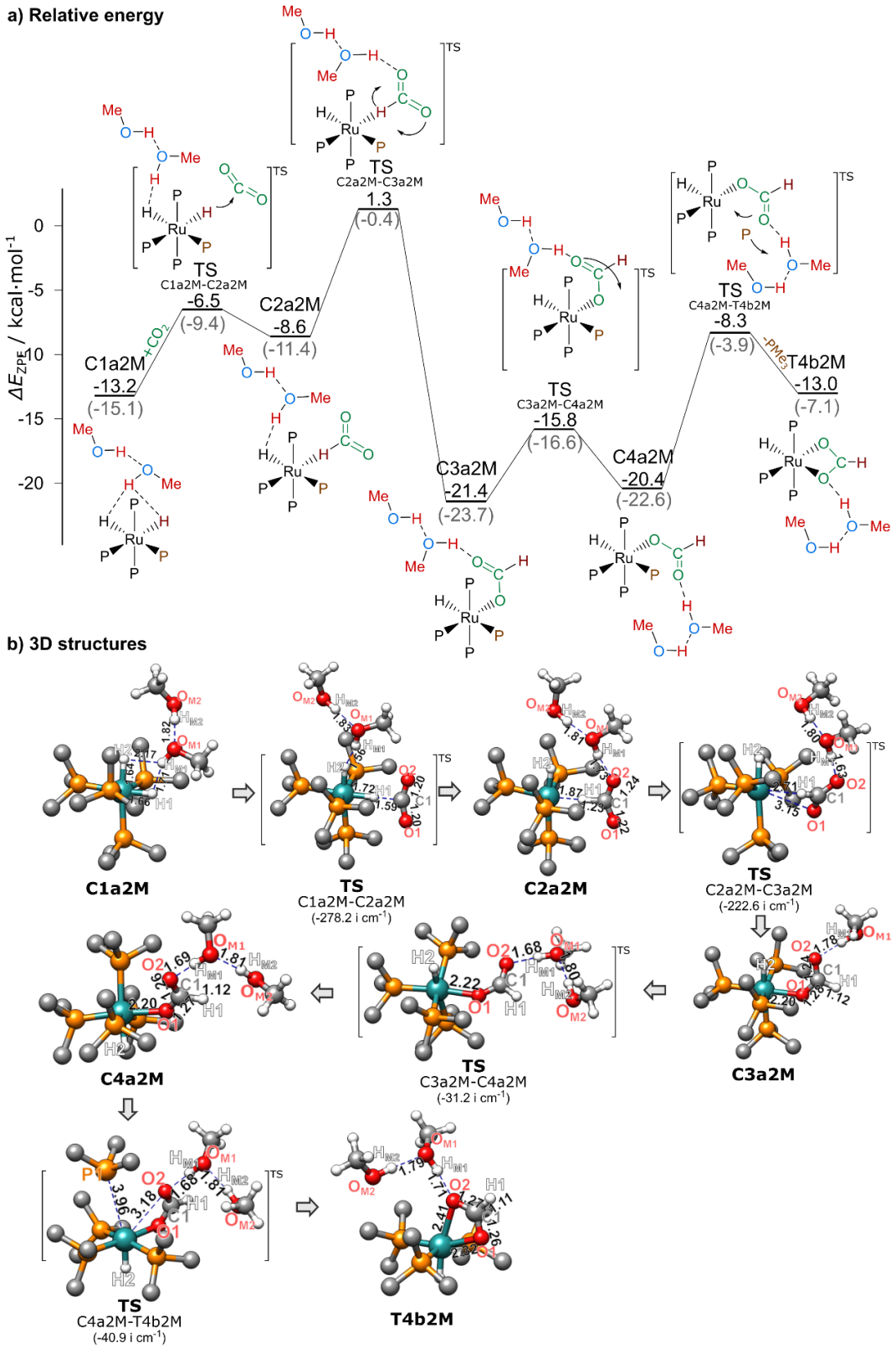

Figure S15. The reaction path for the direct CO_2 insertion into $(PMe_3)_4RuH_2$, leading to the formation of η^2-OOCH complex, with two solvent MeOH. a) Relative Energy for the intermediate and transition structures in kcal/mol, with B3LYP results indicated by black lines and black numbers and PBE0 results in gray parenthesis; b) 3D structures, with the hydrogen atoms on the methyl groups omitted.

5.4.2 CO_2 insertion & intramolecular ligand substitution of $(PMe_3)_3RuH_2(MeOH)\cdot MeOH$

As shown in Figure S16, CO_2 can also direct insert into $(PMe_3)_3RuH_2(MeOH)$ with one solvent MeOH (**CM-C1aM**), and the coordinated methanol can help with this insertion by forming a hydrogen bond, just like the case of $(PMe_3)_3RuH_2(MeOH)$ alone. The barrier of CO_2 insertion into $(PMe_3)_3RuH_2(MeOH)\cdot MeOH$ is 6.4 kcal/mol, which is similar to the case of $(PMe_3)_3RuH_2(MeOH)$ alone, while that of intramolecular substitution of coordinated methanol is reduce to only 0.3 kcal/mol. The η^2-OOCH complex can be formed more easily.

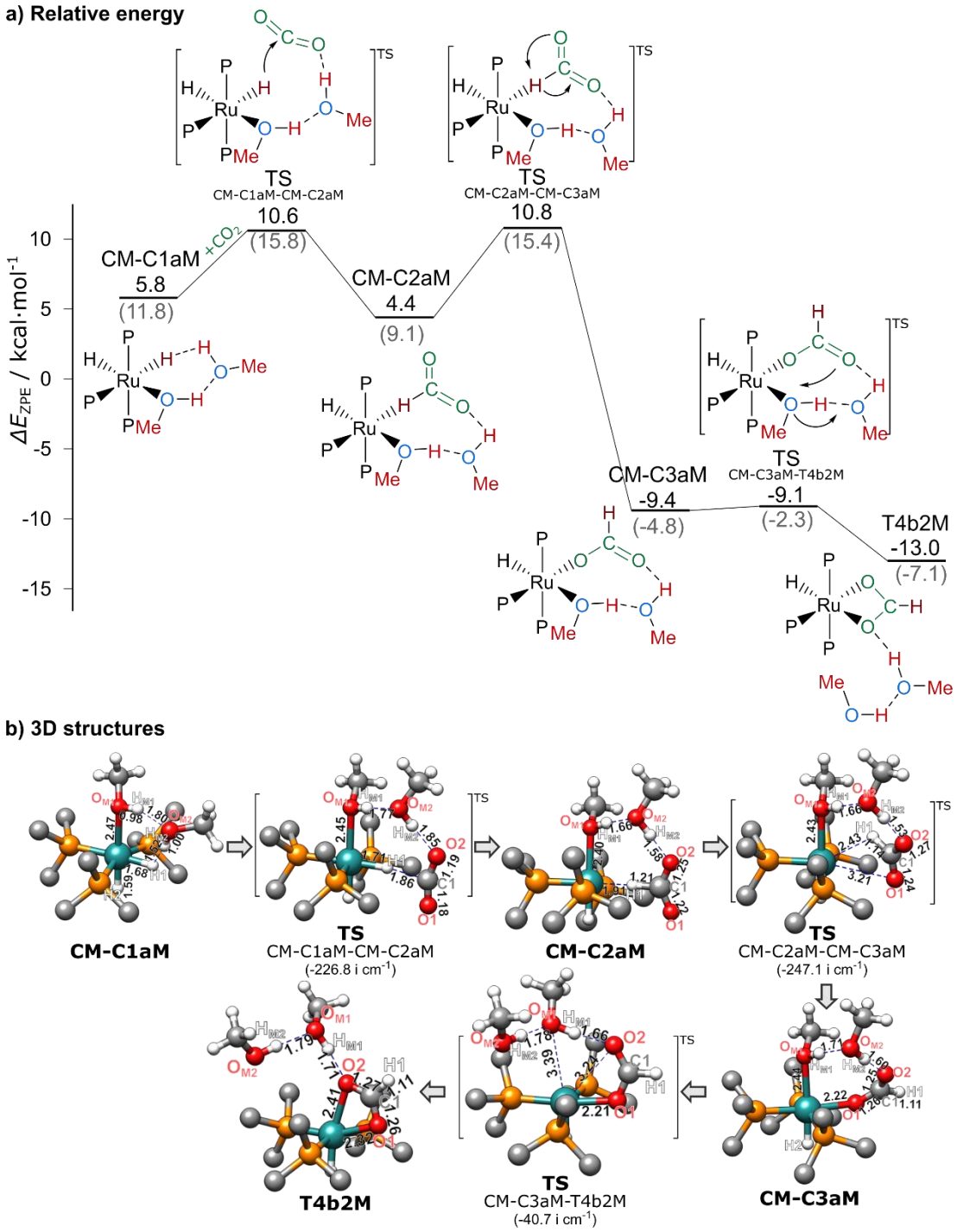

Figure S16. The reaction path for CO_2 insertion into $(PMe_3)_3RuH_2(MeOH)$ in the presence of a solvent MeOH, leading to the formation of η^2-OOCH complex. a) Relative Energy for the intermediate and transition structures in kcal/mol, with B3LYP results indicated by black lines and black numbers and PBE0 results in gray parenthesis; b) 3D structures, with the hydrogen atoms on the methyl groups omitted.

5.4.3 H_2 insertion, metathesis & HCOOH·NMe_3 elimination with two solvent MeOH.

Just like case of two solvent waters, we also calculate all the typical pathway of $\mathbf{2M_N}$, $\mathbf{M_NM_{Rp}}$, $\mathbf{M_R}$ $\mathbf{M_{Rp}}$ and $\mathbf{2M_{Rp}}$, and the favorable pathway is shown in Figure S17. In this pathway, the metathesis follows the $\mathbf{M_RM_{Rp}}$ pathway, while the NMe_3 insertion and elimination of HCOOH·NMe_3 follows $\mathbf{2M_{Rp}}$ pathway.

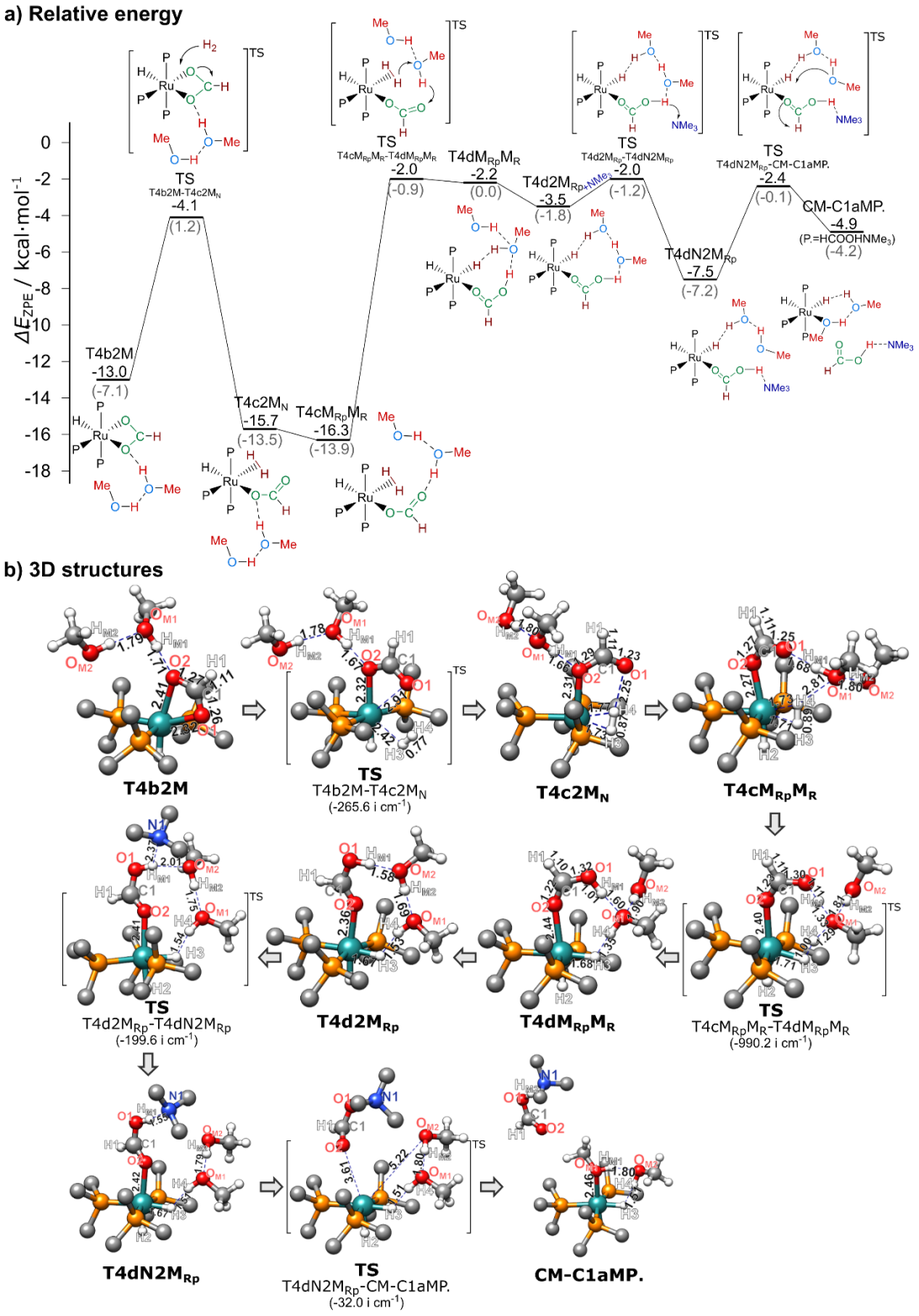

Figure S17. The reaction path for H_2 insertion into $(PMe_3)_3RuH(\eta^2\text{-}OOCH)$ followed by the metathesis and the elimination of $HCOOH{\cdot}NMe_3$, in presence of two MeOH. a) Relative Energy for the intermediate and transition structures in kcal/mol, with B3LYP results indicated by black lines and black numbers and PBE0 results in gray parenthesis; b) 3D structures, with the hydrogen atoms on the methyl groups omitted.

5.5 Reaction of one $NHMe_2$

In the case of $NHMe_2$, only the coordinated pathway (**CA-C1a**) is considered, as the previous study of water and methanol has shown only the solvation of additives will not have an obvious promotion effect on the catalytic reaction. The promotion effect of the additives comes from the more active complex $(PMe_3)_3RuH_2L$, with L=H_2O, MeOH, or $HNMe_2$, which is dynamically generated in the $HCOOH{\cdot}NMe_3$ elimination step.

5.5.1 CO_2 insertion & intramolecular ligand substitution of $(PMe_3)_3RuH_2(NHMe_2)$

As shown in Figure S18, CO_2 can direct insert into $(PMe_3)_3RuH_2(NHMe_2)$ (**CA-C1a**), and the coordinated $NHMe_2$ can help with this insertion by forming a hydrogen bond, just like the case of coordinated water and methanol. The hydrogen bond of 1.85Å in **CA-C2a** is slightly weaker than the case of coordinated water and methanol, which is around 1.5Å. Because this hydrogen bond is weaker as the rotation shaft of $HCOO^-$, the barrier of CO_2 insertion into $(PMe_3)_3RuH_2(MeOH)$ is 9.1 kcal/mol, which is considerably higher than that in the case of coordinated water and methanol. The intramolecular substitution barrier of coordinated $NHMe_2$ is slightly higher with the value of 5.5 kcal/mol, as the $NHMe_2$ binds tighter with Ru than H_2O and MeOH.

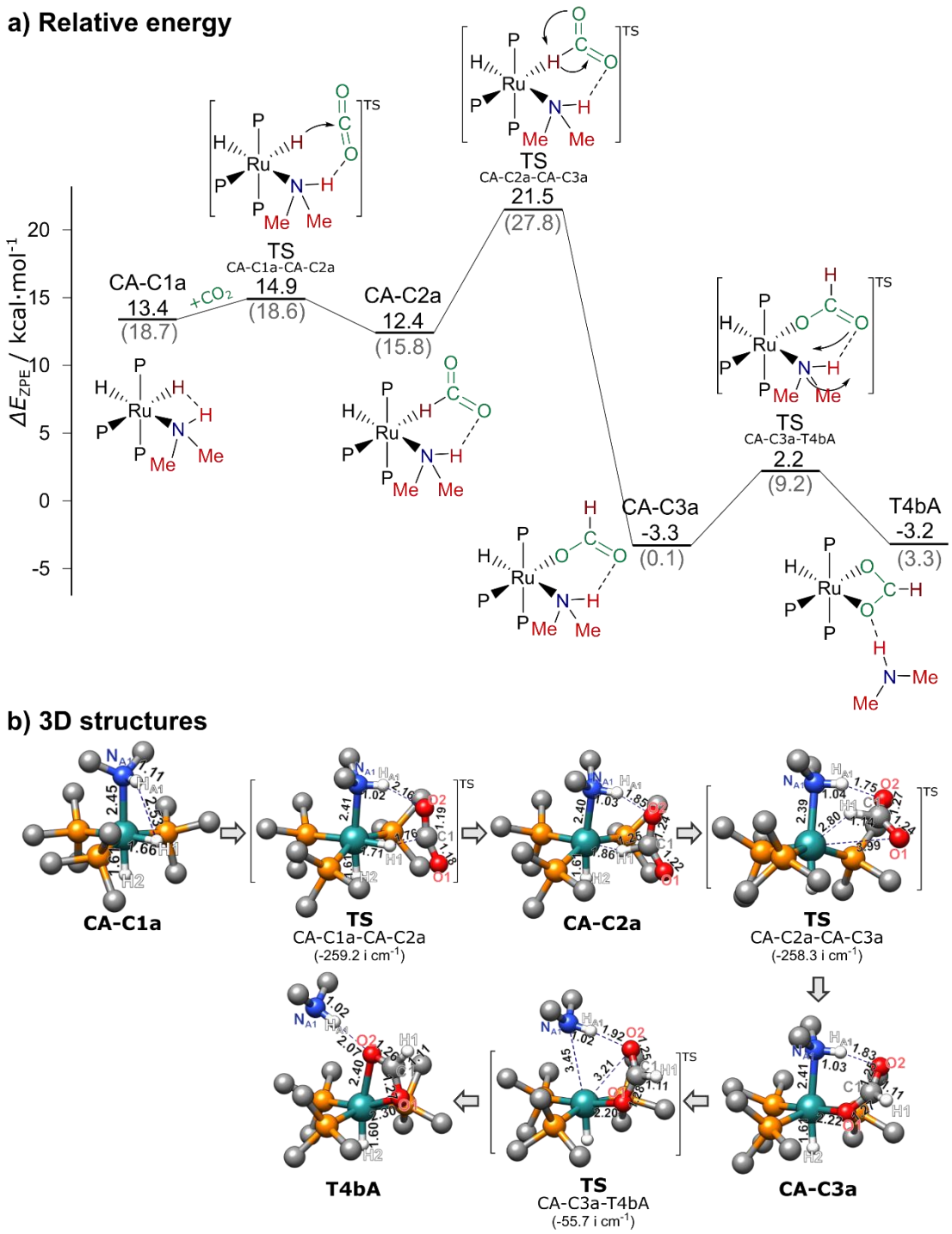

Figure S18. The reaction path for CO_2 insertion into $(PMe_3)_3RuH_2(NHMe_2)$, leading to the formation of η^2-OOCH complex. a) Relative Energy for the intermediate and transition structures in kcal/mol, with B3LYP results indicated by black lines and black numbers and PBE0 results in gray parenthesis; b) 3D structures, with the hydrogen atoms on the methyl groups omitted.

5.5.2 *H_2 insertion, metathesis & HCOOH·$NHMe_2$ elimination with one solvent $NHMe_2$.*

As shown in Figure S19, after the formation of $(PMe_3)_3RuH(\eta^2\text{-}OOCH)$, the following steps of H_2 insertion, metathesis, and HCOOH elimination are also the same with the case of H_2O and MeOH, except that the proton transfer media becomes now $NHMe_2$. Noticing the $NHMe_2$ is both the base and the additive. In the final step of HCOOH·$NHMe_2$ elimination, one extra $NHMe_2$ is added to balance the reaction.

If we compare the reaction cycle of coordinated $NHMe_2$ with that of coordinated H_2O and MeOH, as shown in Table 1, the overall barrier is similar, although the coordinated $NHMe_2$ binds tighter with Ru. This is because neither the TDTS and TDI involve coordinated additive but solvent additive. Hence for such kinds of additives, the aggregation of additive molecules, *i.e.* the dynamical effect in the HCOOH elimination step plays a more important role on the acceleration.

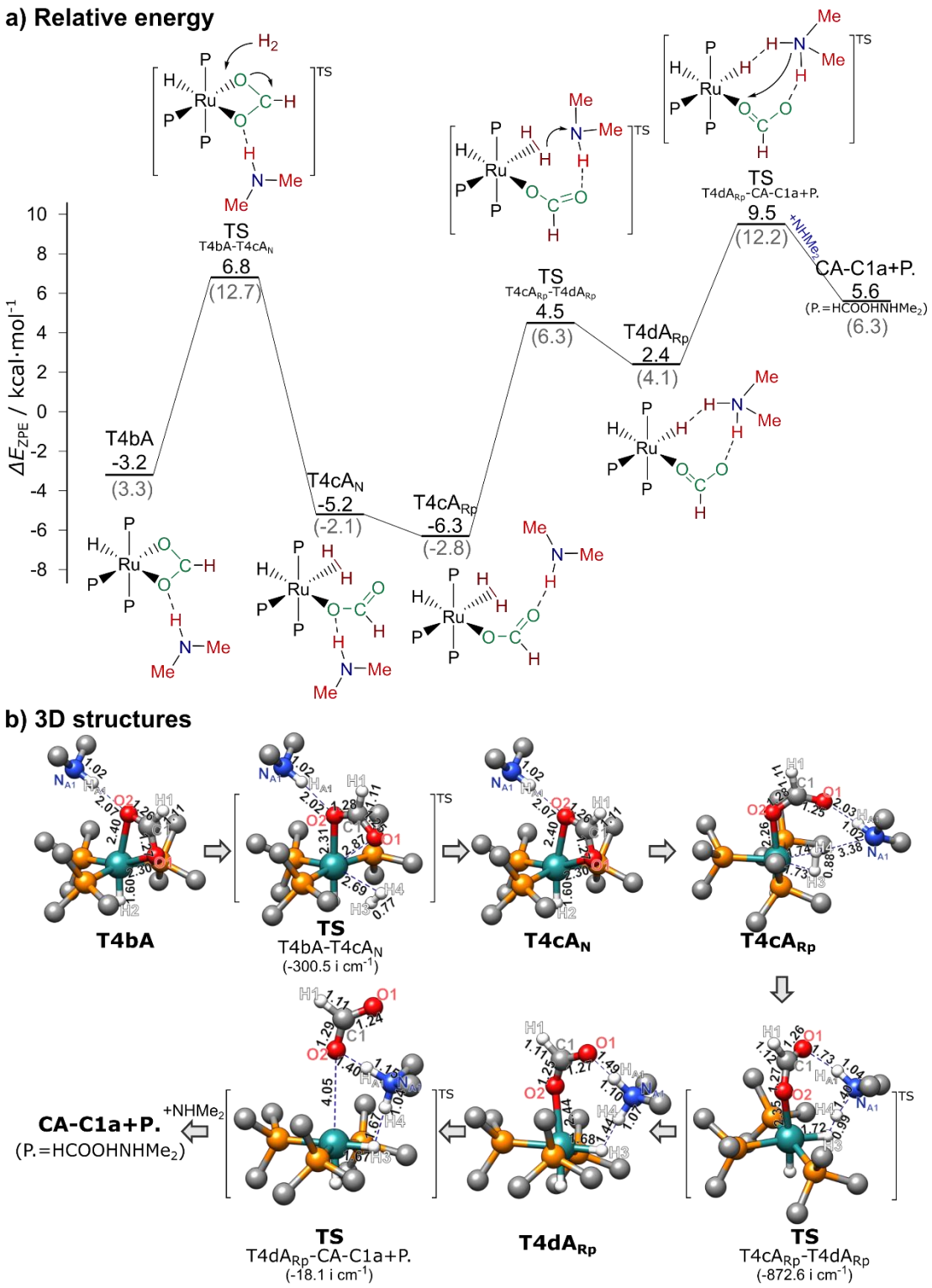

Figure S19. The reaction path for H_2 insertion into $(PMe_3)_3RuH(\eta^2\text{-}OOCH)$ followed by the metathesis and the elimination of $HCOOH{\cdot}NMe_3$, in presence of one solvent $NHMe_2$. a) Relative Energy for the intermediate and transition structures in kcal/mol, with B3LYP results indicated by black lines and black numbers and PBE0 results in gray parenthesis; b) 3D structures, with the hydrogen atoms on the methyl groups omitted.

5.6 Reaction of two $NHMe_2$

5.6.1 CO_2 insertion & intramolecular ligand substitution of $(PMe_3)_3RuH_2(NHMe_2)\cdot NHMe_2$

As shown in Figure S20, CO_2 can also direct insert into $(PMe_3)_3RuH_2(NHMe_2)$ with one solvent $NHMe_2$ (**CA-C1aA**), and the coordinated $NHMe_2$ can help with this insertion by forming a hydrogen bond, just like the case of one coordinated $NHMe_2$. The barrier of CO_2 insertion into $(PMe_3)_3RuH_2(NHMe_2)\cdot NHMe_2$ is 5.9 kcal/mol, which is similar to the case of $(PMe_3)_3RuH_2(NHMe_2)$ alone, while that of intramolecular substitution of coordinated $NHMe_2$ is reduce to only 1.3 kcal/mol. The η^2-OOCH complex can be formed easily.

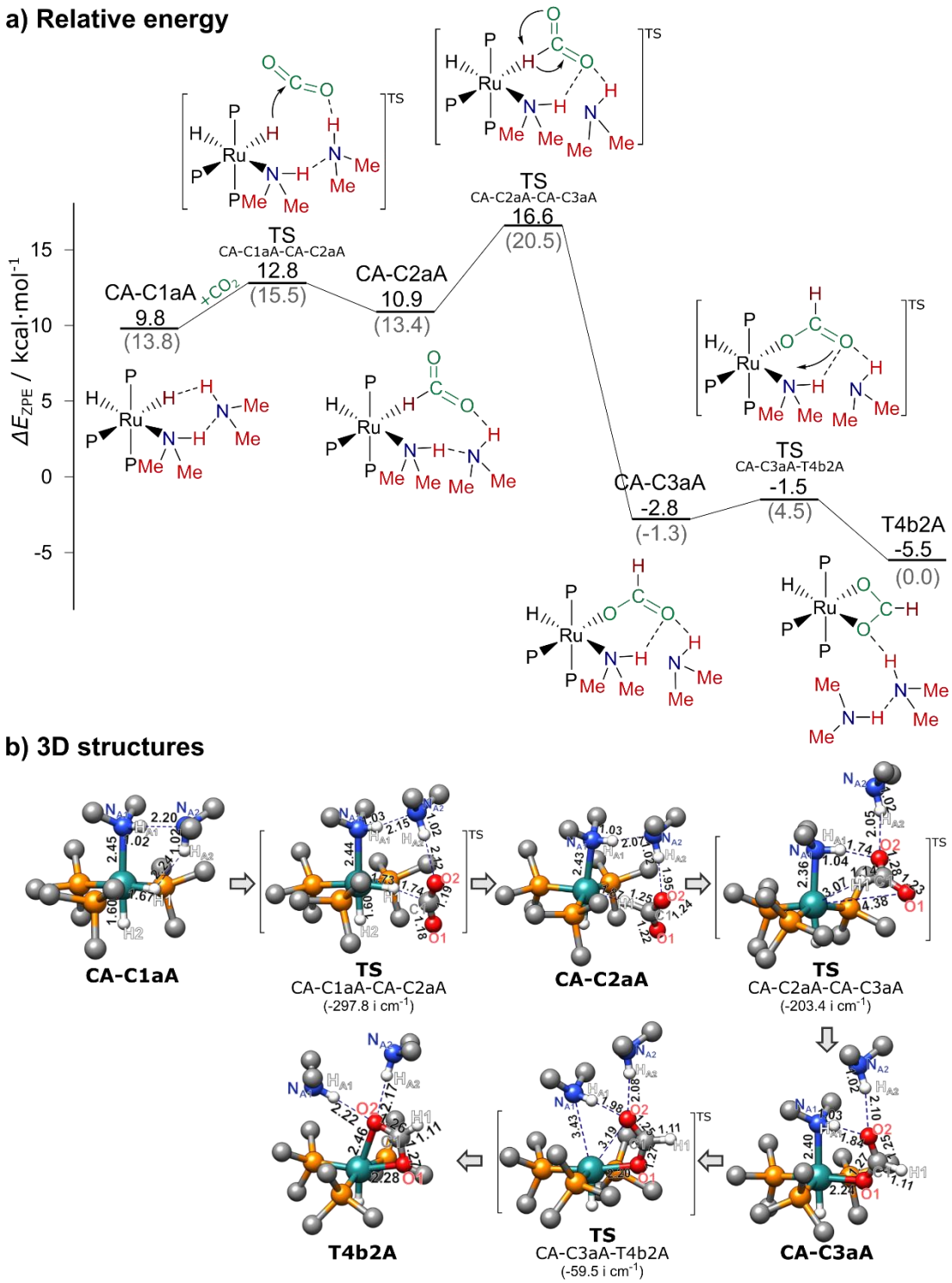

Figure S20. The reaction path for CO_2 insertion into $(PMe_3)_3RuH_2(NHMe_2)$ in presence of one solvent $NHMe_2$, leading to the formation of η^2-OOCH complex. a) Relative Energy for the intermediate and transition structures in kcal/mol, with B3LYP results indicated by black lines and black numbers and PBE0 results in gray parenthesis; b) 3D structures, with the hydrogen atoms on the methyl groups omitted.

5.6.2 H_2 insertion, metathesis & HCOOH·$NHMe_2$ elimination with two solvent $NHMe_2$.

Just like case of two solvent H_2O and MeOH, there also exist different $NHMe_2$ binding sites. As shown in Figure S21, we just follow the favorable reaction pathway here, in which the metathesis follows the $\mathbf{A_RA_{Rp}}$ pathway and the HCOOH·$NHMe_2$ elimination follows the $\mathbf{2M_{Rp}}$ pathway. Noticing the $NHMe_2$ is both the base and the additive. In the final step of HCOOH·$NHMe_2$ elimination, one extra $NHMe_2$ is added to balance the reaction.

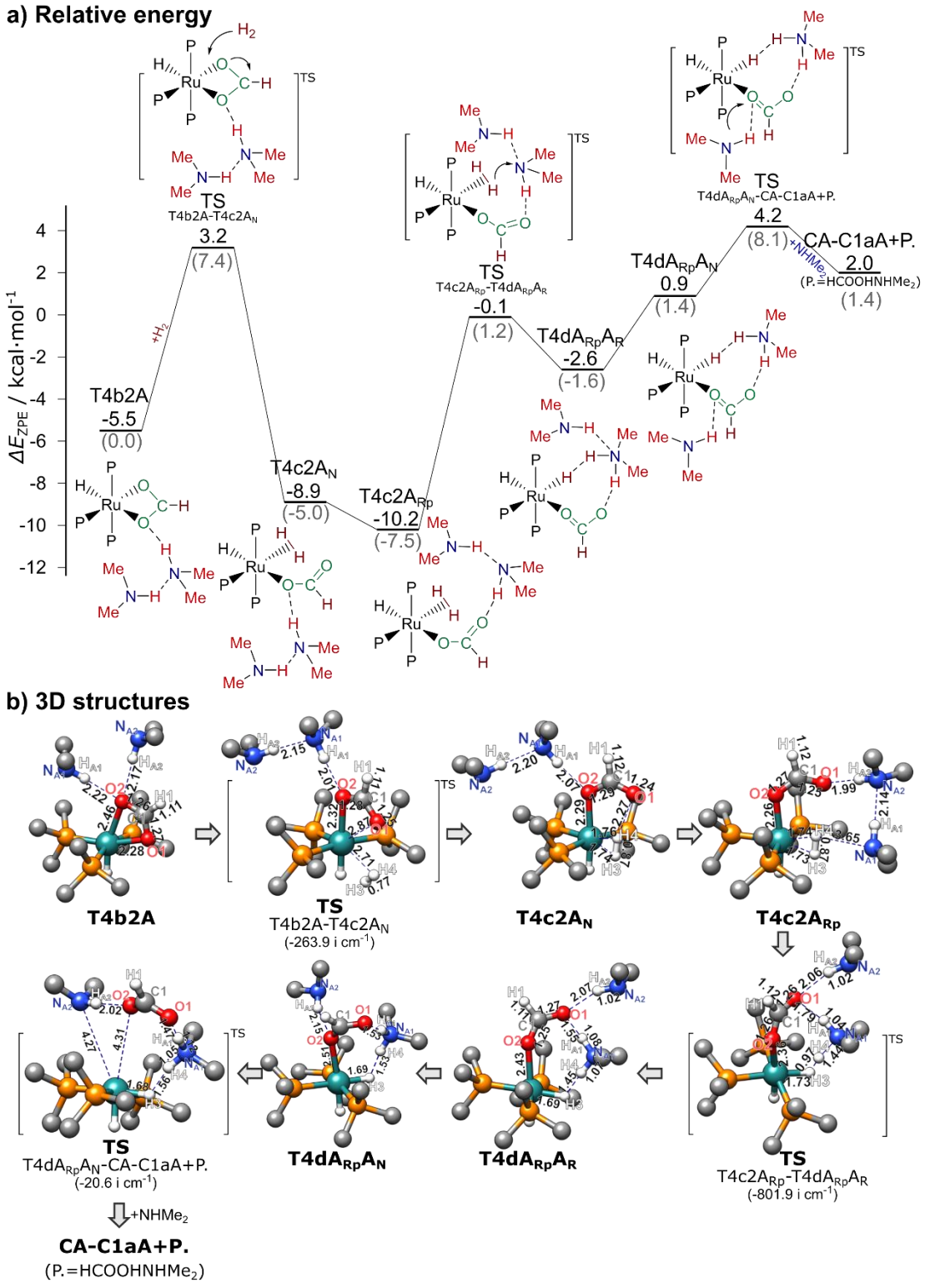

Figure S21. The reaction path for H_2 insertion into $(PMe_3)_3RuH(\eta^2\text{-}OOCH)$ followed by the metathesis and the elimination of $HCOOH{\cdot}NMe_3$, in presence of two solvent $NHMe_2$. a) Relative Energy for the intermediate and transition structures in kcal/mol, with B3LYP results indicated by black lines and black numbers and PBE0 results in gray parenthesis; b) 3D structures, with the hydrogen atoms on the methyl groups omitted.

Reference:

(1) Ohnishi, Y. Y.; Matsunaga, T.; Nakao, Y.; Sato, H.; Sakaki, S. *Journal of the American Chemical Society* **2005**, *127*, 4021.

(2) Ohnishi, Y. Y.; Nakao, Y.; Sato, H.; Sakaki, S. *Organometallics* **2006**, *25*, 3352.

(3) Pomelli, C. S.; Tomasi, J.; Sola, M. *Organometallics* **1998**, *17*, 3164.

(4) Weymuth, T.; Couzijn, E. P.; Chen, P.; Reiher, M. *Journal of chemical theory and computation* **2014**, *10*, 3092.

(5) Jessop, P. G.; Hsiao, Y.; Ikariya, T.; Noyori, R. *Journal of the American Chemical Society* **1996**, *118*, 344.

(6) Xia, G. J.; Liu, J. W.; Liu, Z. F. *Dalton Transactions* **2016**, *45*, 17329.

(7) Munshi, P.; Main, A. D.; Linehan, J. C.; Tai, C. C.; Jessop, P. G. *J. Am. Chem. Soc.* **2002**, *124*, 7963.